Synthetic Benchmarks for Scientific Research in Explainable Machine Learning

Yang Liu[*] [1] **Sujay Khandagale**[*] [1] **Colin White**[1] **Willie Neiswanger**[2]

Abstract

As machine learning models grow more complex and their applications become more high-stakes, tools for explaining model predictions have become increasingly important. Despite the widespread use of explainability techniques, evaluating and comparing different feature attribution methods remains challenging: evaluations ideally require human studies, and empirical evaluation metrics are often computationally prohibitive on real-world datasets. In this work, we address this issue by releasing XAI-BENCH: a suite of synthetic datasets along with a library for benchmarking feature attribution algorithms. Unlike real-world datasets, synthetic datasets allow the efficient computation of conditional expected values that are needed to evaluate ground-truth Shapley values and other metrics. The synthetic datasets we release offer a wide variety of parameters that can be configured to simulate real-world data. We demonstrate the power of our library by benchmarking popular explainability techniques across several evaluation metrics and identifying failure modes for popular explainers. The efficiency of our library will help bring new explainability methods from development to deployment.

1. Introduction

The last decade has seen a huge increase in applications of machine learning in a wide variety of high-stakes domains, such as credit scoring, fraud detection, criminal recidivism, and loan repayment (Mukerjee et al., 2002; Bogen & Rieke, 2018; Ngai et al., 2011; Barocas et al., 2017), and therefore, research on model explainability is becoming increasingly more important. Many different methods for explainability are actively being explored (Fu, 1991; Ribeiro et al., 2016; Lundberg & Lee, 2017; Li et al., 2018; Chen et al., 2018a), The most common type of explainers are post-hoc, local feature attribution methods (Zhang et al., 2020; Lundberg & Lee, 2017; Ribeiro et al., 2016; Plumb et al., 2018; Chen et al., 2018b), which output a set of weights corresponding to the importance of each feature for a given datapoint and model prediction. Currently there are no widely adopted methods to easily *evaluate and/or compare* different feature attribution algorithms. Evaluating the effectiveness of explanations is an intrinsically human-centric task that ideally requires human studies. Although empirical evaluation metrics have been proposed, many of these metrics are computationally prohibitive to compute on real-world datasets. For example, a popular method for feature attribution is to approximate Shapley values (Lundberg & Lee, 2017), but computing the distance to ground-truth Shapley values requires estimating exponentially many conditional feature distributions, which is not possible to compute unless the dataset contains sufficiently many datapoints across exponentially many combinations of features.

In this work, we release a suite of synthetic datasets, which make it possible to efficiently benchmark feature attribution methods. The use of synthetic datasets, for which the ground-truth distribution of data is known, makes it possible to exactly compute the conditional distribution over any set of features, thus enabling computations of many feature attribution evaluation metrics such as distance to ground-truth Shapley values (Lundberg & Lee, 2017), remove-and-retrain (ROAR) (Hooker et al., 2018), faithfulness (Alvarez-Melis & Jaakkola, 2018), and monotonicity (Luss et al., 2019). Our synthetic datasets offer a wide variety of parameters which can be configured to simulate real-world data and have the potential to identify subtle failure modes. We give examples of how real datasets can be converted to similar synthetic datasets, thereby allowing explainability methods to be benchmarked on realistic synthetic datasets.

We showcase the power of our library by benchmarking popular explainers with respect to a broad set of evaluation metrics, across different models and data distribution types. Our library is designed to substantially accelerate the time it takes for researchers and practitioners to move their explainability algorithms from development to deployment. All of our code, API docs, and walkthroughs are available

[*]Equal contribution [1]Abacus.AI [2]Stanford University, Computer Science Department. Correspondence to: Yang Liu <yang@abacus.ai>, Sujay Khandagale <sujay@abacus.ai>.

Accepted to the XAI Workshop at ICML, 2021.

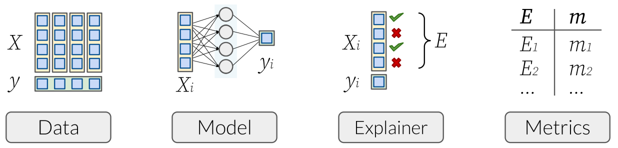

Figure 1. Overview of the main components in XAI-BENCH.

at https://github.com/abacusai/xai-bench.

2. Related Work

Model explainability in machine learning has seen a wide range of approaches. Popular approaches include logic rules (Fu, 1991; Towell & Shavlik, 1993; Setiono & Liu, 1995), hidden semantics (Zhang et al., 2018), feature attribution (Ribeiro et al., 2016; Lundberg & Lee, 2017; Plumb et al., 2018; Chen et al., 2018b; Strumbelj & Kononenko, 2010; Aas et al., 2021), and explanation by example (Li et al., 2018; Chen et al., 2018a). For surveys, see Zhang et al. (2020), Arrieta et al. (2020), Adadi & Berrada (2018), and Došilović et al. (2018).

Some recent works have given experimental surveys of explainability methods using human labeling (Jeyakumar et al., 2020), or two approximate evaluation metrics (Arya et al., 2019). Another recent work (DeYoung et al., 2019) gives a set of benchmark natural language processing (NLP) datasets aimed at comparing explainability methods usin human-annotated explanations. For a more detailed discussion of related work, see Appendix Section B.

3. Evaluation Metrics

In this section, we define several different evaluation metrics for explainability methods. We start with notation and definitions. Given a distribution $\mathcal{D}$, each datapoint is of the form $(\boldsymbol{x}, y) \sim \mathcal{D}$, where $\boldsymbol{x}$ denotes the set of features, and y denotes the label. We assume that $\boldsymbol{x} \in [0,1]^D$ and $y \in [0,1]$, yet all of the concepts we discuss can be generalized to arbitrary categorical and real-valued feature distributions and labels. Assume we have a training set $\mathcal{D}_{\text{train}}$ and a test set $\mathcal{D}_{\text{test}}$, both drawn from $\mathcal{D}$. We train a model $f : [0,1]^D \to [0,1]$ on the training set. A *feature attribution method* is a function g such that, given a model f and a datapoint $\boldsymbol{x}$, $g(\boldsymbol{x}, f) = \boldsymbol{w} \in [-1,1]^D$, where each output weight w_i corresponds to the relative importance of feature i when making the prediction $f(\boldsymbol{x})$.

A *feature attribution evaluation metric* is a function which evaluates a feature attribution method. Many evaluation metrics involve evaluating the change in performance of the model when a subset of features of a datapoint are replaced with background values. Formally, given a datapoint $\boldsymbol{x} \sim \mathcal{D}$ and a set of indices $S \subseteq \{1, \cdots, D\}$, we define $\mathcal{D}(\boldsymbol{x}_S)$ as the conditional probability distribution $\boldsymbol{x}' \sim \mathcal{D}$ such that $x'_i = x_i$ for all $i \in S$. Let $F = \{1, \cdots, D\}$. Given a datapoint $\boldsymbol{x}$, a model f, and a weight vector $\boldsymbol{w}$, the first evaluation metric, faithfulness (**faith-**) (Alvarez-Melis & Jaakkola, 2018), is defined as follows:

$$\text{faith}- = \text{Pearson}\Bigg([w_i]_{1\le i\le D}, \left| \mathbb{E}_{\boldsymbol{x}'\sim\mathcal{D}\left(\boldsymbol{x}_{F\setminus i}\right)}[f(\boldsymbol{x}')] - f(\boldsymbol{x}) \right|_{1\le i\le D} \Bigg).$$

In other words, faith$-$ computes the Pearson correlation coefficient (Wright, 1921) between the weight vector and the approximate marginal contribution of each feature. We also study a new variant of faithfulness: instead of computing the marginal improvement between $\mathcal{D}\left(\boldsymbol{x}_{F\setminus i}\right)$ and $\mathcal{D}\left(\boldsymbol{x}_F\right)$, we compute the marginal improvement between $\mathcal{D}\left(\boldsymbol{x}_\emptyset\right)$ and $\mathcal{D}\left(\boldsymbol{x}_{\{i\}}\right)$. We call this variant **faith+**. The next metric, monotonicity (**mono-**), (Luss et al., 2019), computes the marginal improvement of each feature ordered by the weight vector $\boldsymbol{w}$ *without replacement*, and then computes the fraction of indices i such that the marginal improvement for feature i is greater than the marginal improvement for feature $i+1$. Similar to faithfulness, we define a new variant, **mono+**, by computing in the opposite order. See Appendix G.1 for the formal description.

The types of metrics discussed so far each require computing f on different combinations of features, and it is possible that these combinations of features have very low density in $\mathcal{D}$, and are therefore unlikely to occur in $\mathcal{D}_{\text{train}}$, making the evaluations on f unreliable. To help mitigate this issue, another paradigm of explainability evaluation metrics was proposed: remove-and-retrain (ROAR) (Hooker et al., 2018). In this paradigm, in order to evaluate the marginal improvement of sets of features, the model is retrained using a new dataset with the features removed. The original work reported a plot for each explainer (Hooker et al., 2018). In order to report a scalar metric, we propose four new metrics by combining the remove-and-retrain paradigm with faithfulness and monotonicity: **roar-faith+/-** and **roar-mono+/-**. That is, the definitions are similar to faith+/- and mono+/-, but f is replaced with the retrained model as defined above, accordingly. See Appendix G.1 for the formal definitions.

A caveat for all of the aforementioned metrics is that they evaluate each feature weight by computing the effect of removing the feature from a single set of features S. Another type of metric uses *Shapley values* (Lundberg & Lee, 2017; Datta et al., 2016; Lipovetsky & Conklin, 2001; Strumbelj & Kononenko, 2010), which take into account the marginal improvement of a feature i across *all possible* sets with and without i. We consider two Shapley-based metrics: **shapley-mse** and **shapley-corr**, which involve computing the ground-truth Shapley values (Lundberg & Lee, 2017) for each feature, and then computing either the mean squared error (MSE) or Pearson correlation, respectively, between

Table 1. Summary of evaluation metrics.

Metric	Type	Evaluations	Retrain	Linearity
faith+/-	correlation	$\Theta(D)$		✓
mono+/-	ranking	$\Theta(D)$		✓
roar-faith+/-	correlation	$\Theta(D)$	✓	✓
roar-mono+/-	ranking	$\Theta(D)$	✓	✓
shapley-mse	accuracy	$\Theta(2^D)$		
shapley-corr	correlation	$\Theta(2^D)$		

the weight vector and the set of ground-truth Shapley values. See Table 1 for a summary of the properties of each metric. Researchers may use any or all of the above metrics for evaluating and comparing different feature attribution explaination techniques. The metric to rely on the most depends on the specific use-case, dataset, feature attribution technique, or computational constraints. We give more discussion in Appendix G.1.

4. Synthetic Datasets

In this section, we describe the synthetic datasets used in our library. We start by discussing the benefits of synthetic datasets when evaluating feature attribution methods.

The case for synthetic data As shown in Section 3, key to the metrics is computing the conditional expectation $\mathbb{E}_{\boldsymbol{x}'\sim\mathcal{D}(\boldsymbol{x}_S)}[f(\boldsymbol{x}')]$ for a subset S, datapoint $\boldsymbol{x}$, and trained model f. On real-world datasets, the conditional distribution $\mathcal{D}(\boldsymbol{x}_S)$ can only be approximated, and the approximation may be very poor when the conditional distribution defines a low-dimensional region of the feature space. Since all evaluation metrics require computing $\Theta(D)$ or $\Theta(2^D)$ such expectations, for each datapoint $\boldsymbol{x}$, is is likely that some evaluations will make use of a poor approximation. However, for the synthetic datasets that we define, the conditional distributions are known, allowing exact computation of the evaluation metrics. Additionally, as we show in Section 5, synthetic datasets allow one to explicitly control all attributes of the dataset, which allows for targeted experiments, for example, investigating explainer performance as a function of feature correlation. For explainers such as SHAP (Lundberg & Lee, 2017) which assume feature independence, this type of experiment may be very beneficial.

Feature distributions Now we describe the synthetic datasets in our library. The generation is split into two parts, generating features $\boldsymbol{x}$, and defining a function to generate labels y from $\boldsymbol{x}$. For feature generation, we consider both multivariate normal distributions, and mixture of Gaussian distributions. For a multivariate normal distribution of a D-dimensional random vector, we set $\boldsymbol{X} \sim \mathcal{N}(\boldsymbol{\mu}, \boldsymbol{\Sigma})$, where $\boldsymbol{\mu}$ is the $\boldsymbol{D}$-dimensional mean vector, and $\boldsymbol{\Sigma}$ is the $\boldsymbol{D} \times \boldsymbol{D}$ covariance matrix. $\boldsymbol{\mu}$ can take any value, and $\boldsymbol{\Sigma}$ must be symmetric and positive definite. In Appendix E, we show how to efficiently compute the conditional distribution for any datapoint and set of feature indices, using $\boldsymbol{\mu}$ and $\boldsymbol{\Sigma}$. We include the description for the multivariate Gaussian feature distribution in Appendix F.

Label distributions Next, we compute the distribution of labels. The distributions we implement are `linear`, `piecewise constant`, and `nonlinear additive`. Data labels are computed from features, i.e., $y_{\text{raw}} = \sum_{n=1}^{D} \Psi_n(x_n)$ where Ψ_n is a function that operates on feature n. For `linear` datasets, $\Psi_n(x_n)$ are scalar weights, and we can rewrite the raw labels as $y_{raw} = \boldsymbol{w}^T\boldsymbol{x}$. For `piecewise constant` datasets, $\Psi_n(x_n)$ are piecewise constant functions made up of different threshold values (similar to Aas et al. (2021)). For `nonlinear additive` datasets, $\Psi_n(x_n)$ are nonlinear functions including *absolute*, *cosine*, and *exponent* function adapted from Chen et al. (2018b). Detailed specifications can be found in Appendix H.

5. Experiments

In this section, we describe our experiments in benchmarking several popular feature attribution methods across synthetic datasets. We compare six different feature attribution methods: SHAP (Lundberg & Lee, 2017), SHAPR (Aas et al., 2021), brute-force Kernel SHAP (BF-SHAP) (Lundberg & Lee, 2017), LIME (Ribeiro et al., 2016), MAPLE (Plumb et al., 2018), and L2X (Chen et al., 2018b). We also compare the methods to RANDOM explainer, which outputs random weights drawn from a standard normal distribution. See Appendix G for descriptions and implementation details for all methods. We report mean and standard deviation from three trials for all experiments.

First, we run experiments using the normalized multivariate Gaussian dataset ($\boldsymbol{\mu}$ set to 0, the diagonal of $\boldsymbol{\Sigma}$ set to 1, and the non-diagonal terms set to 0) with `piecewise constant` labels. As shown in Table 2, the relative performance of explainers varies dramatically across metrics for a fixed decision tree model. SHAP, BF-SHAP, SHAPR, and LIME offer accurate approximation of ground truth Shapley values (> 0.9 shapley-corr). In addition, LIME achieves top performance in three out of four ROAR-based metrics. Unexpectedly, none of the explainers outperformed random on mono-, suggesting that this metric is not helpful for this dataset and model. Another surprising observation is that while MAPLE performs well for faith+/-, and roar-mono+/-, it fails for roar-faith+/- by producing large negative scores.

Next, we compare the performance of the explainers as a function of feature correlation (varying ρ, the non-diagonal terms of the covariance matrix $\boldsymbol{\Sigma}$). As shown in Figure 2, a general trend is that explainers become worse as feature correlation increases. Explainers such as SHAP assume feature

Table 2. Explainer performance across metrics. All performance numbers are from explaining a multilayer perceptron trained on the Gaussian piecewise constant dataset with $\rho = 0$.

	RANDOM	SHAP	BF-SHAP	SHAPR	LIME	MAPLE	L2X
faith+(↑)	$-0.028_{\pm 0.022}$	$\mathbf{0.922}_{\pm 0.020}$	$0.887_{\pm 0.031}$	$0.918_{\pm 0.039}$	$0.859_{\pm 0.035}$	$0.626_{\pm 0.050}$	$-0.004_{\pm 0.100}$
faith-(↑)	$-0.022_{\pm 0.023}$	$0.970_{\pm 0.006}$	$0.937_{\pm 0.017}$	$\mathbf{0.977}_{\pm 0.004}$	$0.918_{\pm 0.010}$	$0.647_{\pm 0.045}$	$0.002_{\pm 0.080}$
mono+(↑)	$0.538_{\pm 0.012}$	$\mathbf{0.720}_{\pm 0.018}$	$0.676_{\pm 0.027}$	$0.719_{\pm 0.019}$	$0.667_{\pm 0.032}$	$0.712_{\pm 0.008}$	$0.562_{\pm 0.024}$
mono-(↑)	$\mathbf{0.467}_{\pm 0.006}$	$0.433_{\pm 0.019}$	$0.449_{\pm 0.027}$	$0.435_{\pm 0.012}$	$0.428_{\pm 0.014}$	$0.440_{\pm 0.017}$	$0.430_{\pm 0.040}$
roar-faith+(↑)	$0.003_{\pm 0.028}$	$0.461_{\pm 0.095}$	$0.496_{\pm 0.016}$	$0.468_{\pm 0.082}$	$\mathbf{0.585}_{\pm 0.046}$	$-0.429_{\pm 0.018}$	$0.045_{\pm 0.060}$
roar-faith-(↑)	$0.008_{\pm 0.049}$	$0.581_{\pm 0.024}$	$0.535_{\pm 0.067}$	$0.559_{\pm 0.026}$	$\mathbf{0.621}_{\pm 0.019}$	$-0.339_{\pm 0.013}$	$0.052_{\pm 0.038}$
roar-mono+(↑)	$0.474_{\pm 0.016}$	$0.747_{\pm 0.028}$	$\mathbf{0.771}_{\pm 0.015}$	$0.730_{\pm 0.022}$	$0.707_{\pm 0.024}$	$0.425_{\pm 0.009}$	$0.500_{\pm 0.027}$
roar-mono-(↑)	$0.492_{\pm 0.019}$	$0.721_{\pm 0.032}$	$0.683_{\pm 0.038}$	$0.713_{\pm 0.044}$	$\mathbf{0.745}_{\pm 0.020}$	$0.471_{\pm 0.016}$	$0.451_{\pm 0.041}$
shapley-corr(↑)	$0.001_{\pm 0.014}$	$0.992_{\pm 0.005}$	$0.956_{\pm 0.007}$	$\mathbf{0.998}_{\pm 0.001}$	$0.955_{\pm 0.009}$	$0.735_{\pm 0.038}$	$0.073_{\pm 0.084}$
shapley-mse(↓)	$1.134_{\pm 0.040}$	$0.003_{\pm 0.001}$	$0.008_{\pm 0.001}$	$\mathbf{0.000}_{\pm 0.000}$	$0.026_{\pm 0.001}$	$0.071_{\pm 0.007}$	$0.188_{\pm 0.022}$

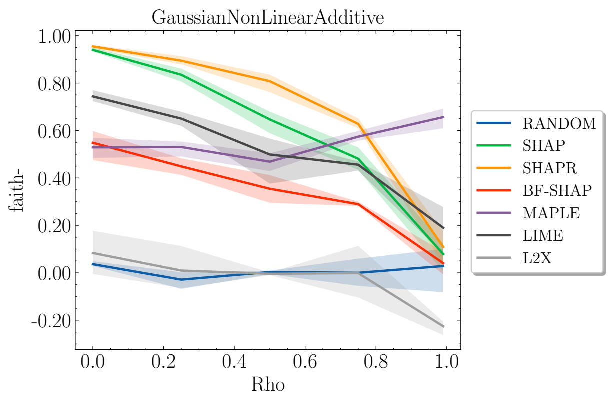

Figure 2. Results for faith- on a multilayer perceptron on a Gaussian nonlinear additive label distribution.

independence and tend to perform well when features are indeed independent ($\rho = 0$), but decline for higher values of ρ. On the other hand, MAPLE's performance stayed relatively stable. In Appendix G.1, we run an exhaustive set of experiments using different datasets and models.

Next, we demonstrate the power and flexibility of synthetic datasets by simulating the popular wine dataset (Cortez et al., 2009; Staniak & Biecek, 2018) with synthetic features so that it can be used to efficiently benchmark feature attribution methods. This dataset has 11 continuous features and a categorical label. The features are first normalized to have zero mean and unit variance, then an empirical covariance matrix is computed, which is then used as the input covariance matrix to generate synthetic multivariate Gaussian features. Simulated wine quality is labeled by a k-nearest neighbor model based on real datapoints. We compute the Jensen-Shannon Divergence (JSD) (Wong & You, 1985) of the real and synthetic wine datasets, to be 0.20. Since this number is close to zero, it suggests a good fit. We also train three models on both simulated and real wine datasets and compare the MSE of explanations on a common held-out real test set. As shown in Appendix Table 5, consistent low MSE across ML models and explainers suggest that the simulated dataset is a good proxy for the original wine dataset for evaluating explainers. We evaluate the explainers on the synthetic dataset in Appendix Section J.

Recommended usage Throughout Section 5, we gave a sample of the types of experiments that can be done using XAI-BENCH (recall that our comprehensive experiments are in Appendix G.1). For researchers looking to develop new explainability techniques, we recommend benchmarking new algorithms across all metrics using our synthetic datasets with different values of ρ. These datasets give a good initial picture of the efficacy of new techniques. For researchers with a dataset and application in mind, we recommend converting the dataset into a synthetic dataset using the technique described in the previous paragraph. Note that converting to a synthetic dataset also gives the ability to evaluate explainability techniques on perturbations of the original covariance matrix, to simulate robustness to distribution shift. Finally, researchers can decide on the evaluation metric that is most suitable to the application at hand, based on the model, intended use-case, size and number of features of the dataset, and level of feature correlation. We give more discussion in Appendix G.1.

6. Conclusion

In this work, we released a set of synthetic datasets along with a library for benchmarking feature attribution algorithms. The use of synthetic datasets with known ground-truth distributions makes it possible to exactly compute the conditional distribution over any set of features, enabling computations of several explainability evaluation metrics, including ground-truth Shapley values, ROAR, faithfulness, and monotonicity. Our synthetic datasets offer a variety of parameters which can be configured to simulate real-world data and have the potential to identify failure modes of explainability techniques. We showcase the power of our library by benchmarking several popular explainers with respect to ten evaluation metrics across a variety of settings.

Acknowledgments

WN was supported by U.S. Department of Energy Office of Science under Contract No. DE-AC02-76SF00515.

References

Aas, K., Jullum, M., and Løland, A. Explaining individual predictions when features are dependent: More accurate approximations to shapley values. *Artificial Intelligence*, pp. 103502, 2021.

Adadi, A. and Berrada, M. Peeking inside the black-box: a survey on explainable artificial intelligence (xai). *IEEE access*, 6:52138–52160, 2018.

Alvarez-Melis, D. and Jaakkola, T. S. Towards robust interpretability with self-explaining neural networks. *arXiv preprint arXiv:1806.07538*, 2018.

Ancona, M., Oztireli, C., and Gross, M. Explaining deep neural networks with a polynomial time algorithm for shapley value approximation. In *International Conference on Machine Learning*, pp. 272–281. PMLR, 2019.

Arrieta, A. B., Díaz-Rodríguez, N., Del Ser, J., Bennetot, A., Tabik, S., Barbado, A., García, S., Gil-López, S., Molina, D., Benjamins, R., et al. Explainable artificial intelligence (xai): Concepts, taxonomies, opportunities and challenges toward responsible ai. *Information Fusion*, 58:82–115, 2020.

Arya, V., Bellamy, R. K., Chen, P.-Y., Dhurandhar, A., Hind, M., Hoffman, S. C., Houde, S., Liao, Q. V., Luss, R., Mojsilović, A., et al. One explanation does not fit all: A toolkit and taxonomy of ai explainability techniques. *arXiv preprint arXiv:1909.03012*, 2019.

Barocas, S., Hardt, M., and Narayanan, A. Fairness in machine learning. *NIPS Tutorial*, 2017.

Bogen, M. and Rieke, A. Help wanted: An examination of hiring algorithms, equity, and bias, 2018.

Chattopadhay, A., Sarkar, A., Howlader, P., and Balasubramanian, V. N. Grad-cam++: Generalized gradient-based visual explanations for deep convolutional networks. In *2018 IEEE Winter Conference on Applications of Computer Vision (WACV)*, pp. 839–847. IEEE, 2018.

Chen, C., Li, O., Tao, C., Barnett, A. J., Su, J., and Rudin, C. This looks like that: deep learning for interpretable image recognition. *arXiv preprint arXiv:1806.10574*, 2018a.

Chen, J., Song, L., Wainwright, M., and Jordan, M. Learning to explain: An information-theoretic perspective on model interpretation. In *International Conference on Machine Learning*, pp. 883–892. PMLR, 2018b.

Cortez, P., Cerdeira, A., Almeida, F., Matos, T., and Reis, J. Modeling wine preferences by data mining from physicochemical properties. *Decision support systems*, 47(4): 547–553, 2009.

Datta, A., Sen, S., and Zick, Y. Algorithmic transparency via quantitative input influence: Theory and experiments with learning systems. In *2016 IEEE symposium on security and privacy (SP)*, pp. 598–617. IEEE, 2016.

Denton, E., Hutchinson, B., Mitchell, M., and Gebru, T. Detecting bias with generative counterfactual face attribute augmentation. *arXiv preprint arXiv:1906.06439*, 2019.

DeYoung, J., Jain, S., Rajani, N. F., Lehman, E., Xiong, C., Socher, R., and Wallace, B. C. Eraser: A benchmark to evaluate rationalized nlp models. *arXiv preprint arXiv:1911.03429*, 2019.

Došilović, F. K., Brčić, M., and Hlupić, N. Explainable artificial intelligence: A survey. In *2018 41st International convention on information and communication technology, electronics and microelectronics (MIPRO)*, pp. 0210–0215. IEEE, 2018.

Fauvel, K., Masson, V., and Fromont, E. A performance-explainability framework to benchmark machine learning methods: Application to multivariate time series classifiers. *arXiv preprint arXiv:2005.14501*, 2020.

Fu, L. Rule learning by searching on adapted nets. In *AAAI*, volume 91, pp. 590–595, 1991.

Heskes, T., Sijben, E., Bucur, I. G., and Claassen, T. Causal shapley values: Exploiting causal knowledge to explain individual predictions of complex models. *arXiv preprint arXiv:2011.01625*, 2020.

Hooker, S., Erhan, D., Kindermans, P.-J., and Kim, B. A benchmark for interpretability methods in deep neural networks. *arXiv preprint arXiv:1806.10758*, 2018.

Jeyakumar, J. V., Noor, J., Cheng, Y.-H., Garcia, L., and Srivastava, M. How can i explain this to you? an empirical study of deep neural network explanation methods. *Advances in Neural Information Processing Systems*, 2020.

Lage, I., Ross, A. S., Kim, B., Gershman, S. J., and Doshi-Velez, F. Human-in-the-loop interpretability prior. *arXiv preprint arXiv:1805.11571*, 2018.

Larson, J., Mattu, S., Kirchner, L., and Angwin, J. How we analyzed the compas recidivism algorithm. *ProPublica (5 2016)*, 9, 2016.

Li, O., Liu, H., Chen, C., and Rudin, C. Deep learning for case-based reasoning through prototypes: A neural network that explains its predictions. In *Proceedings of the*

AAAI Conference on Artificial Intelligence, volume 32, 2018.

Lipovetsky, S. and Conklin, M. Analysis of regression in game theory approach. *Applied Stochastic Models in Business and Industry*, 17(4):319–330, 2001.

Lundberg, S. M. and Lee, S.-I. A unified approach to interpreting model predictions. *Advances in Neural Information Processing Systems*, 30:4765–4774, 2017.

Luss, R., Chen, P.-Y., Dhurandhar, A., Sattigeri, P., Zhang, Y., Shanmugam, K., and Tu, C.-C. Generating contrastive explanations with monotonic attribute functions. *arXiv preprint arXiv:1905.12698*, 2019.

Mukerjee, A., Biswas, R., Deb, K., and Mathur, A. P. Multi–objective evolutionary algorithms for the risk–return trade–off in bank loan management. *International Transactions in operational research*, 2002.

Ngai, E. W., Hu, Y., Wong, Y. H., Chen, Y., and Sun, X. The application of data mining techniques in financial fraud detection: A classification framework and an academic review of literature. *Decision support systems*, 50(3): 559–569, 2011.

Pineau, J., Vincent-Lamarre, P., Sinha, K., Larivière, V., Beygelzimer, A., d'Alché Buc, F., Fox, E., and Larochelle, H. Improving reproducibility in machine learning research (a report from the neurips 2019 reproducibility program). *arXiv preprint arXiv:2003.12206*, 2020.

Plumb, G., Molitor, D., and Talwalkar, A. Model agnostic supervised local explanations. *arXiv preprint arXiv:1807.02910*, 2018.

Ribeiro, M. T., Singh, S., and Guestrin, C. " why should i trust you?" explaining the predictions of any classifier. In *Proceedings of the 22nd ACM SIGKDD international conference on knowledge discovery and data mining*, 2016.

Ribeiro, M. T., Singh, S., and Guestrin, C. Anchors: High-precision model-agnostic explanations. In *Proceedings of the AAAI Conference on Artificial Intelligence*, volume 32, 2018.

Ross, A. and Doshi-Velez, F. Improving the adversarial robustness and interpretability of deep neural networks by regularizing their input gradients. In *Proceedings of the AAAI Conference on Artificial Intelligence*, volume 32, 2018.

Selvaraju, R. R., Cogswell, M., Das, A., Vedantam, R., Parikh, D., and Batra, D. Grad-cam: Visual explanations from deep networks via gradient-based localization. In *Proceedings of the IEEE international conference on computer vision*, pp. 618–626, 2017.

Setiono, R. and Liu, H. Understanding neural networks via rule extraction. In *IJCAI*, volume 1, pp. 480–485. Citeseer, 1995.

Simonyan, K., Vedaldi, A., and Zisserman, A. Deep inside convolutional networks: Visualising image classification models and saliency maps. *arXiv preprint arXiv:1312.6034*, 2013.

Staniak, M. and Biecek, P. Explanations of model predictions with live and breakdown packages. *arXiv preprint arXiv:1804.01955*, 2018.

Strumbelj, E. and Kononenko, I. An efficient explanation of individual classifications using game theory. *The Journal of Machine Learning Research*, 11:1–18, 2010.

Towell, G. G. and Shavlik, J. W. Extracting refined rules from knowledge-based neural networks. *Machine learning*, 13(1):71–101, 1993.

Wong, A. K. and You, M. Entropy and distance of random graphs with application to structural pattern recognition. *IEEE Transactions on Pattern Analysis and Machine Intelligence*, 1985.

Wright, S. Correlation and causation. *Journal of Agricultural Research*, 20:557–580, 1921.

Zhang, Q., Wu, Y. N., and Zhu, S.-C. Interpretable convolutional neural networks. In *Proceedings of the IEEE Conference on Computer Vision and Pattern Recognition*, pp. 8827–8836, 2018.

Zhang, Y., Tiňo, P., Leonardis, A., and Tang, K. A survey on neural network interpretability. *arXiv preprint arXiv:2012.14261*, 2020.

A. Societal Impact

Machine learning models are more prevalent now than ever before. With the widespread deployment of models in applications that impact human lives, explainability is becoming increasingly more important for the purposes of debugging, legal obligations, and mitigating bias (Lundberg & Lee, 2017; Zhang et al., 2020; Arya et al., 2019; DeYoung et al., 2019). Given the importance of high-quality explanations, it is essential that the explainability methods are reliable across all types of datasets. Our work seeks to speed up the development of explainability methods, with a focus on catching edge cases and failure modes, to ensure that new explainability methods are robust before they are used in the real world. Of particular importance are improving the reliability of explainability methods intended to recognize biased predictions, for example, ensuring that the features used to predict criminal recidivism are not based on race or gender (Larson et al., 2016). Frameworks for evaluating and comparing explainability methods are an important part of creating inclusive and unbiased technology. As pointed out in prior work (Denton et al., 2019), while methods for explainability or debiasing are important, they must be part of a larger, socially contextualized project to examine the ethical considerations of the machine learning application.

B. Related Work Continued

Model explainability in machine learning has seen a wide range of approaches, and multiple taxonomies have been proposed to classify the different types of approaches. Zhang et al. (2020) describe three dimensions of explainability techniques: passive/active, type of explanation, and local/global explanations. The types of explanations they identified are logic rules (Fu, 1991; Towell & Shavlik, 1993; Setiono & Liu, 1995), hidden semantics (Zhang et al., 2018), feature attribution (Ribeiro et al., 2016; Lundberg & Lee, 2017; Plumb et al., 2018; Chen et al., 2018b; Strumbelj & Kononenko, 2010; Aas et al., 2021), and explanation by example (Li et al., 2018; Chen et al., 2018a). Other surveys on explainable AI include Arrieta et al. (2020), Adadi & Berrada (2018), and Došilović et al. (2018).

Techniques for feature attribution include approximating Shapley values (Lundberg & Lee, 2017; Datta et al., 2016; Lipovetsky & Conklin, 2001; Strumbelj & Kononenko, 2010), approximating the model locally with a more explainable model (Ribeiro et al., 2016), and approximating the mutual information of each feature with the label (Chen et al., 2018b). In Appendix G, we give descriptions and implementation details of the five feature attribution methods we implemented.

B.1. Benchmarking Explainability Techniques

One recent work (Jeyakumar et al., 2020) gave an experimental survey of explainability methods, testing SHAP (Lundberg & Lee, 2017), LIME (Ribeiro et al., 2016), Anchors (Ribeiro et al., 2018), Saliency Maps (Simonyan et al., 2013), and Grad-CAM++ (Chattopadhay et al., 2018), and their proposed ExMatchina on image, text, audio, and sensory datasets. They use human labeling via Mechanical Turk as an evaluation metric. Another work (Arya et al., 2019) gave an experimental survey of several algorithms including local/global, white-box/black-box, and supervised/unsupervised techniques. The only feature attribution algorithms they tested were SHAP and LIME. Another recent work gives a benchmark on explainability for time-series classification (Fauvel et al., 2020). Another recent work (DeYoung et al., 2019) gives a set of benchmark natural language processing (NLP) datasets aimed at comparing explainability methods. This work releases multiple datsets with human-annotated explanations, as well as a few newly proposed metrics specifically chosen to capture the explainability of predictions in NLP applications. To the best of our knowledge, no prior work has released a library with five different evaluation metrics or released a set of synthetic datasets for explainability with more than one tunable parameter.

B.2. Explainability evaluation metrics

While the "correctness" of feature attribution methods may be subjective, comparisons between methods are often based on human studies (Lage et al., 2018; Ross & Doshi-Velez, 2018; Selvaraju et al., 2017). However, human studies are not always possible, and several empirical (non-human) evaluation metrics have been proposed. Faithfulness (Alvarez-Melis & Jaakkola, 2018) measures the correlation between the weights of the feature attribution algorithm, and the effect of the features on the performance of the model. Monotonicity (Luss et al., 2019) checks whether iteratively adding features from least weighted feature to most weighted feature, causes the prediction to monotonically improve. By retraining a model with subsets of features ablated, ROAR (Hooker et al., 2018) uses a new model with partially ablated input features to evaluate a feature attribution technique while avoiding problems with distribution shift. Note that all of the above metrics evaluate feature importance by computing the effect of removing the feature from a single set of features S. In contrast, Shapley values (Lundberg & Lee, 2017; Datta et al., 2016; Lipovetsky & Conklin, 2001; Strumbelj & Kononenko, 2010) evaluate all possible sets S that a feature can be removed from to compute an average effect.

C. Dataset Documentation and Intended Use

Our code is available at https://github.com/abacusai/xai-bench.

C.1. Author responsibility

We bear all responsibility in case of violation of rights, etc. The license of our repository is the **Apache License 2.0**. For more information, see https://github.com/abacusai/xai-bench/blob/main/LICENSE.

C.2. Maintenance plan and contributing policy.

We plan to actively maintain the repository, and we welcome contributions from the explainability community and machine learning community at large. For more information, see https://github.com/abacusai/xai-bench. As our benchmarks are synthetic, we will host the code to generate the datasets on GitHub.

C.3. Code of conduct

Our Code of Conduct is adapted from the Contributor Covenant, version 2.0, available at
https://www.contributor-covenant.org/version/2/0/code_of_conduct.html.
The policy is copied below.

> "We as members, contributors, and leaders pledge to make participation in our community a harassment-free experience for everyone, regardless of age, body size, visible or invisible disability, ethnicity, sex characteristics, gender identity and expression, level of experience, education, socio-economic status, nationality, personal appearance, race, caste, color, religion, or sexual identity and orientation."

D. Reproducibility Checklist

To ensure reproducibility, we use the Machine Learning Reproducibility Checklist v2.0, Apr. 7, 2020 (Pineau et al., 2020). An earlier version of this checklist (v1.2) was used for NeurIPS 2019 (Pineau et al., 2020).

- For all **models** and **algorithms** presented,
  - **A clear description of the mathematical setting, algorithm, and/or model.** We clearly describe all of the settings and algorithms in Section 5 and Appendix Section G.
  - **A clear explanation of any assumptions.** Some of the explainability techniques implemented in our repository make assumptions about the dataset (e.g., that all features are independent). We give this information in Appendix G.
  - **An analysis of the complexity (time, space, sample size) of any algorithm.** We compute the complexity analysis in Section 3 and Appendix Section G.
- For any **theoretical claim**,
  - **A clear statement of the claim.** We do not make theoretical claims.
  - **A complete proof of the claim.** We do not make theoretical claims.
- For all **datasets** used, check if you include:
  - **The relevant statistics, such as number of examples.** We used a real dataset in Section 5. We give the statistics for this dataset in the same section.
  - **The details of train / validation / test splits** We give this information in our repository.
  - **An explanation of any data that were excluded, and all pre-processing step.** We did not exclude any data or perform any preprocessing.
  - **A link to a downloadable version of the dataset or simulation environment.** Our repository contains all of the instructions to download and run experiments on the datasets in our work. See https://github.com/abacusai/xai-bench.
  - **For new data collected, a complete description of the data collection process, such as instructions to annotators and methods for quality control.** We release new synthetic datasets, so there was no collection process. The code to generate the synthetic datasets is hosted on GitHub.
- For all shared **code** related to this work, check if you include:
  - **Specification of dependencies.** We give installation instructions in the README of our repository.
  - **Training code.** The training code is available in our repository.
  - **Evaluation code.** The training code is available in our repository.
  - **(Pre-)trained model(s).** We do not release any pre-trained models. The code to run all experiments in our work can be found in the GitHub repository.
  - **README file includes table of results accompanied by precise command to run to produce those results.** We include a README with detailed instructions to reproduce our experiments.

- For all reported **experimental results**, check if you include:
  - **The range of hyper-parameters considered, method to select the best hyper-parameter configuration, and specification of all hyper-parameters used to generate results.** We use default configuration for explainers except SHAPR, tuning details in Appendix G.2
  - **The exact number of training and evaluation runs.** We report 3 runs for each experiment.
  - **A clear definition of the specific measure or statistics used to report results.** We define our metrics in Section 3 and Appendix G.1.
  - **A description of results with central tendency (e.g. mean) & variation (e.g. error bars).** We report mean and standard deviation for all experiments.
  - **The average runtime for each result, or estimated energy cost.** We report the runtimes in Section J.
  - **A description of the computing infrastructure used.** We use CPUs for all experiments. We give details of our experiments in Appendix Section J.

E. Multivariate Gaussian distribution

The multivariate normal distribution of a $\boldsymbol{D}$-dimensional random vector $\boldsymbol{X} = (X_1, ..., X_D)^T$ can be written as $\boldsymbol{X} \sim \mathcal{N}(\boldsymbol{\mu}, \boldsymbol{\Sigma})$, where $\boldsymbol{\mu}$ is the $\boldsymbol{D}$-dimensional mean vector, and $\boldsymbol{\Sigma}$ is the $\boldsymbol{D} \times \boldsymbol{D}$ covariance matrix. Without loss of generality, we can partition the $\boldsymbol{D}$-dimensional vector $\boldsymbol{x}$ as $\boldsymbol{X} = (\boldsymbol{X}_1, \boldsymbol{X}_2)^T$. To compute the distribution of $\boldsymbol{X}_1$ conditional on $\boldsymbol{X_2} = \boldsymbol{x_2^*}$ where $\boldsymbol{x_2^*}$ is a $\boldsymbol{K}$-dimensional vector with $0 < \boldsymbol{K} < \boldsymbol{D}$, we can then partition $\boldsymbol{\mu}$ and $\boldsymbol{\Sigma}$ accordingly:

$$\boldsymbol{\mu} = \begin{bmatrix} \boldsymbol{\mu}_1 \\ \boldsymbol{\mu}_2 \end{bmatrix}, \quad \boldsymbol{\Sigma} = \begin{bmatrix} \boldsymbol{\Sigma}_{11} & \boldsymbol{\Sigma}_{12} \\ \boldsymbol{\Sigma}_{21} & \boldsymbol{\Sigma}_{22} \end{bmatrix}.$$

Then the conditional distribution is a new multivariate normal $(\boldsymbol{X}_1 | \boldsymbol{X}_2 = \boldsymbol{x}_2^*) \sim \mathcal{N}(\boldsymbol{\mu}^*, \boldsymbol{\Sigma}^*)$ where

$$\boldsymbol{\mu}^* = \boldsymbol{\mu}_1 + \boldsymbol{\Sigma}_{12}\boldsymbol{\Sigma}_{22}^{-1}(\boldsymbol{x}_2^* - \boldsymbol{\mu}_2), \tag{1}$$

$$\boldsymbol{\Sigma}^* = \boldsymbol{\Sigma}_{11} + \boldsymbol{\Sigma}_{12}\boldsymbol{\Sigma}_{22}^{-1}\boldsymbol{\Sigma}_{21}. \tag{2}$$

For any $\boldsymbol{x}_2^* \in \mathbb{R}^K$, one can compute $\boldsymbol{\mu}^*$ and $\boldsymbol{\Sigma}^*$ and then generate samples from the conditional distribution. $\boldsymbol{\mu}$ can take any value, and $\boldsymbol{\Sigma}$ must be symmetric and positive definite.

The probability density function of a non-degenerative multivariate normal distribution is

$$f_x(x_1, ..., x_D) = \frac{\exp(-\frac{1}{2}(\boldsymbol{x} - \boldsymbol{\mu})^T \boldsymbol{\Sigma}^{-1}(\boldsymbol{x} - \boldsymbol{\mu}))}{\sqrt{(2\pi)^D |\boldsymbol{\Sigma}|}}, \tag{3}$$

with parameters $\boldsymbol{\mu} \in \mathbb{R}^D$ and $\boldsymbol{\Sigma} \in \mathbb{R}^{D \times D}$.

F. Mixture of Gaussian features

Now we describe the mixture of Gaussian features. Suppose now that $\boldsymbol{X} = (X_1, ..., X_D)^T$ is a $\boldsymbol{D}$-dimensional random vector distributed as a mixture of k Gaussians. We write this as $\boldsymbol{X} \sim \sum_{j=1}^k \pi_j \mathcal{N}(\boldsymbol{\mu}_j, \boldsymbol{\Sigma}_j)$, where each $\boldsymbol{\mu}_j$ is a $\boldsymbol{D}$-dimensional mean vector for the j^{th} mixture component, and $\boldsymbol{\Sigma}_j$ is the $\boldsymbol{D} \times \boldsymbol{D}$ covariance matrix for the j^{th} mixture component.

Suppose, as before we use the partition defined by $\boldsymbol{X} = \begin{bmatrix} \boldsymbol{X}_1 \\ \boldsymbol{X}_2 \end{bmatrix}$ and partition the parameters of each mixture component accordingly as

$$\boldsymbol{\mu}_j = \begin{bmatrix} \boldsymbol{\mu}_{j,1} \\ \boldsymbol{\mu}_{j,2} \end{bmatrix}, \boldsymbol{\Sigma}_j = \begin{bmatrix} \boldsymbol{\Sigma}_{j,11} & \boldsymbol{\Sigma}_{j,12} \\ \boldsymbol{\Sigma}_{j,21} & \boldsymbol{\Sigma}_{j,22} \end{bmatrix}$$

for $j = 1, \ldots, k$. Then, given $X_2 = \boldsymbol{x}_2^*$, the conditional distribution is also a mixture of Gaussians, written $(\boldsymbol{X}_1 | X_2 = \boldsymbol{x}_2^*) \sim \sum_{j=1}^k \pi_j^* \mathcal{N}(\boldsymbol{\mu}_j^*, \boldsymbol{\Sigma}_j^*)$, where the parameters of each mixture component can be written

$$\boldsymbol{\mu_j^*} = \boldsymbol{\mu}_{j,1} + \boldsymbol{\Sigma}_{j,12}\boldsymbol{\Sigma}_{j,22}^{-1}(\boldsymbol{x}_2^* - \boldsymbol{\mu}_{j,2}) \tag{4}$$

$$\boldsymbol{\Sigma_j^*} = \boldsymbol{\Sigma}_{j,11} + \boldsymbol{\Sigma}_{j,12}\boldsymbol{\Sigma}_{j,22}^{-1}\boldsymbol{\Sigma}_{j,21} \tag{5}$$

$$\pi_j^* = \frac{\pi_j f_{j,2}(\boldsymbol{x}_2^*)}{\sum_{\ell=1}^k \pi_\ell f_{\ell,2}(\boldsymbol{x}_2^*)} \tag{6}$$

and where $f_{j,2}$ denotes the probability density function of the multivariate normal distribution $\mathcal{N}(\mu_{j,2}, \Sigma_{j,22})$.

G. Descriptions of Explainability Metrics and Explainers

G.1. Metrics

In this section, we give the formal definitions for the rest of the evaluation metrics from Section 3. We start by formally defining the monotonicity metrics.

Formally, define $S^-(\boldsymbol{w}, i)$ as the set of i least important weights, define $S^+(\boldsymbol{w}, i)$ as the set of i most important weights, and let $S^-(\boldsymbol{w}, 0) = \emptyset$. Given a datapoint $\boldsymbol{x}$, a model f, and a weight vector $\boldsymbol{w}$, we define **monotonicity** (mono$-$) (Luss et al., 2019) as follows:

$$\begin{aligned} \delta_i^- &= \mathbb{E}_{\boldsymbol{x'} \sim \mathcal{D}\left(\boldsymbol{x}_{S^-(\boldsymbol{w}, i+1)}\right)}[f(\boldsymbol{x'})] \\ &\quad - \mathbb{E}_{\boldsymbol{x'} \sim \mathcal{D}\left(\boldsymbol{x}_{S^-(\boldsymbol{w}, i)}\right)}[f(\boldsymbol{x'})], \\ \text{mono}- &= \frac{1}{D-1} \sum_{i=0}^{D-2} \mathbb{I}_{|\delta_i^-| \le |\delta_{i+1}^-|}. \end{aligned}$$

Similar to faithfulness, we define a new variant of monotonicity by computing in the opposite order.

Similar to the definition of mono- defined in Section 3, we define mono+ as follows.

$$\begin{aligned}\delta_i^+ &= \mathbb{E}_{\boldsymbol{x}'\sim\mathcal{D}\left(\boldsymbol{x}_{S^+(\boldsymbol{w},i+1)}\right)}[f(\boldsymbol{x}')] \\ &\quad - \mathbb{E}_{\boldsymbol{x}'\sim\mathcal{D}\left(\boldsymbol{x}_{S^+(\boldsymbol{w},i)}\right)}[f(\boldsymbol{x}')], \\ \text{mono+} &= \frac{1}{D-1}\sum_{i=0}^{D-2}\mathbb{I}_{|\delta_i^+|\le|\delta_{i+1}^+|}.\end{aligned}$$

Now we give the definition of the ROAR-based metrics. Recall that the major difference between ROAR-based metrics and other metrics is that in order to evaluate the marginal improvement of sets of features, ROAR-based metrics retrain the model using a new dataset with the features removed. For example, rather than computing $\left|\mathbb{E}_{\boldsymbol{x}'\sim\mathcal{D}\left(\boldsymbol{x}_{F\setminus i}\right)}[f(\boldsymbol{x}')] - f(\boldsymbol{x})\right|$, we would compute $\left|f^*(\mathbb{E}_{\boldsymbol{x}'\sim\mathcal{D}\left(\boldsymbol{x}_{F\setminus i}\right)}[\boldsymbol{x}']) - f(\boldsymbol{x})\right|$, where f^* denotes a model that has been trained on a modification of $\mathcal{D}_{\text{train}}$ where each datapoint has its i features with highest weight removed. Given a datapoint $\boldsymbol{x}$ and a set of features $S\subseteq F$, we start by defining $\bar{\boldsymbol{x}}_S$, the expected value of a datapoint conditioned on the features S from $\boldsymbol{x}$:

$$\bar{\boldsymbol{x}}_S = \begin{cases} x_i \text{ if } i\in S \\ \mathbb{E}\left[x_i' \mid \boldsymbol{x}'\sim\mathcal{D} \text{ s.t. } x_j' = x_j \forall j\in S\right] \text{ if } i\notin S\end{cases}$$

Let $\mathcal{D}_{\text{train}}^{i-}$ denote a new training set by replacing each $\boldsymbol{x}\sim\mathcal{D}_{\text{train}}$ with $\bar{\boldsymbol{x}}_{F\setminus o^-(\boldsymbol{w}(\boldsymbol{x}),i)}$, where $\boldsymbol{w}(\boldsymbol{x})$ denotes the weight vector for $\boldsymbol{x}$ and $o^-(\boldsymbol{w}(\boldsymbol{x}),i)$ denotes the ith most important feature for $\boldsymbol{x}$ according to $\boldsymbol{w}$. That is, $\mathcal{D}_{\text{train}}^{i-}$ is the training set modified by removing the ith most important features for each datapoint. Let f^{i-} denote the model f retrained on $\mathcal{D}_{\text{train}}^{i-}$ instead of $\mathcal{D}_{\text{train}}$. Then we define **roar-faith-** as follows:

$$\text{roar-faith-} = \texttt{Pearson}\left(\left|f^{i-}(\bar{\boldsymbol{x}}_{F\setminus i}) - f(\boldsymbol{x})\right|_{1\le i\le D}, \\ [w_i]_{1\le i\le D}\right),$$

Next, let $\mathcal{D}_{\text{train}}^{i+}$ denote a new training set by replacing each $\boldsymbol{x}\sim\mathcal{D}_{\text{train}}$ with $\bar{\boldsymbol{x}}_{F\setminus o^+(\boldsymbol{w}(\boldsymbol{x}),i)}$, where $\boldsymbol{w}(\boldsymbol{x})$ denotes the weight vector for $\boldsymbol{x}$ and $o^+(\boldsymbol{w}(\boldsymbol{x}),i)$ denotes the ith most important feature for $\boldsymbol{x}$ according to $\boldsymbol{w}$. That is, $\mathcal{D}_{\text{train}}^{i+}$ is the training set modified by removing the ith most important features for each datapoint. Let f^{i+} denote the model f retrained on $\mathcal{D}_{\text{train}}^{i+}$ instead of $\mathcal{D}_{\text{train}}$. Similar to roar-faith-, we define **roar-faith+** as follows:

$$\text{roar-faith+} = \texttt{Pearson}\left(\left|f^{i+}(\bar{\boldsymbol{x}}_{\{i\}}) - f^{i+}(\bar{\boldsymbol{x}}_{\emptyset})\right|_{1\le i\le D}, \\ [w_i]_{1\le i\le D},\right)$$

Recall from Section 3 that $S^-(\boldsymbol{w},i)$ denotes the set of i least important weights, $S^+(\boldsymbol{w},i)$ denotes the set of i most important weights, and $S^-(\boldsymbol{w},0)=\emptyset$. Let $\mathcal{D}_{\text{train}}^{S(k)-}$ denote a new training set by replacing each $\boldsymbol{x}\sim\mathcal{D}_{\text{train}}$ with $\bar{\boldsymbol{x}}_{F\setminus S^-(\boldsymbol{w}(\boldsymbol{x}),k)}$, where $\boldsymbol{w}(\boldsymbol{x})$ denotes the weight vector for $\boldsymbol{x}$. That is, $\mathcal{D}_{\text{train}}^{k-}$ is the training set modified by removing the k least important features for each datapoint. Let $f^{S(k)-}$ denote the model f retrained on $\mathcal{D}_{\text{train}}^{S(k)-}$ instead of $\mathcal{D}_{\text{train}}$. We define **roar-mono-** as follows:

$$\begin{aligned}\bar{\delta}_i^- &= f^{S(k)-}(\bar{\boldsymbol{x}}_{S_{i+1}^-(\boldsymbol{w})}) - f^{S_i^-}(\bar{\boldsymbol{x}}_{S_i^-(\boldsymbol{w})}), \\ \text{roar-mono-} &= \frac{1}{D-1}\sum_{i=0}^{D-2}\mathbb{I}_{|\delta_i^-|\le|\bar{\delta}_{i+1}^-|}\end{aligned}$$

Similarly, let $\mathcal{D}_{\text{train}}^{S(k)+}$ denote a new training set by replacing each $\boldsymbol{x}\sim\mathcal{D}_{\text{train}}$ with $\bar{\boldsymbol{x}}_{F\setminus S^+(\boldsymbol{w}(\boldsymbol{x}),k)}$, where $\boldsymbol{w}(\boldsymbol{x})$ denotes the weight vector for $\boldsymbol{x}$. That is, $\mathcal{D}_{\text{train}}^{k+}$ is the training set modified by removing the k most important features for each datapoint. Let $f^{S(k)+}$ denote the model f retrained on $\mathcal{D}_{\text{train}}^{S(k)+}$ instead of $\mathcal{D}_{\text{train}}$. We define **roar-mono+** as follows:

$$\begin{aligned}\bar{\delta}_i^+ &= f^{S(k)+}(\bar{\boldsymbol{x}}_{S_{i+1}^+(\boldsymbol{w})}) - f^{S(k)+}(\bar{\boldsymbol{x}}_{S_i^+(\boldsymbol{w})}), \\ \text{roar-mono+} &= \frac{1}{D-1}\sum_{i=0}^{D-2}\mathbb{I}_{|\delta_i^+|\le|\bar{\delta}_{i+1}^+|}\end{aligned}$$

Now we give the formal definition for Shapley values. Given a datapoint $\boldsymbol{x}$, the Shapley value v_i is defined as follows.

$$v_i = \sum_{S\subseteq F\setminus\{i\}}\frac{|S|!(|F|-|S|-1)!}{|F|!} \\ \cdot\left(\mathbb{E}_{\boldsymbol{x}'\sim\mathcal{D}\left(\boldsymbol{x}_{S\cup\{i\}}\right)}[f(\boldsymbol{x}')] - \mathbb{E}_{\boldsymbol{x}'\sim\mathcal{D}(\boldsymbol{x}_S)}[f(\boldsymbol{x}')]\right).$$

Then for a datapoint $\boldsymbol{x}$, shapley-corr is defined as the correlation between the weight vector $\boldsymbol{w}$ and the set of Shapley values for $\boldsymbol{x}$, and shapley-mse is defined as the mean squared error between the weight vector $\boldsymbol{w}$ and the set of Shapley values for $\boldsymbol{x}$. Formally,

$$\begin{aligned}\text{shapley-corr} &= \texttt{Pearson}\left([v_i]_{1\le i\le D}, [w_i]_{1\le i\le D}\right), \\ \text{shapley-mse} &= \sum_{i=1}^{D}(v_i - w_i)^2.\end{aligned}$$

The main drawback of this metric is its time complexity, which is $\Theta(2^D)$ for a D-dimensional dataset. Computation quickly becomes infeasible as D scales up.

Researchers may use any or all of the above metrics for evaluating and comparing different feature attribution explaination techniques. The metric to rely on the most depends on the specific use-case, dataset, feature attribution technique, or computational constraints. For example, researchers evaluating Shapley-based methods such as Kernel-SHAP (Lundberg & Lee, 2017), SHAPR (Aas et al., 2021), or other SHAP variants (Strumbelj & Kononenko, 2010; Ancona et al., 2019; Heskes et al., 2020), may wish to use the shapley-mse and shapley-corr metrics. However, the runtime of these metrics is exponential in the number of features. For tasks involving highly structured data such as image data, ROAR-based metrics may perform better because the faithfulness and monotonicity may compute the function in low-density areas. For tasks involving high-dimensional data and a large cost to retrain the model, faithfulness and monotonicity will be much less computationally intensive than ROAR-based or Shapley-based metrics.

G.2. Local Feature Attribute Explainers

In this section, we give descriptions and implementation details of all of the explainability methods and metrics implemented in our library.

G.2.1. SHAP

Lundberg & Lee (2017) proposed a few methods such as BF-SHAP to estimate Shapley values. Due to the unavailability of the generative model of conditional distribution for real datasets, one can not accurately compute $\mathbb{E}[f_S(\boldsymbol{x}_S)]$. BF-SHAP makes two assumptions: (1) model linearity, which makes $\mathbb{E}[f_S(\boldsymbol{x}_S)] = f_S(\mathbb{E}[\boldsymbol{x}_S])$, (2) feature independence assumption: $\mathbb{E}[\boldsymbol{x}_S]$ with **marginal** expectation instead of **conditional** expectation. In this work, we refer the official implementation of SHAP as SHAP, and re-implemented brute-force kernel SHAP as BF-SHAP.

G.2.2. SHAPR

Aas et al. (2021) proposes several techniques to relax both assumptions and improve BF-SHAP such as "Gaussian", "copula", and "empirical". Because the "empirical" method with a fixed σ performs well across tasks in the original paper, we re-implemented the original R package in python with a tuned from $\{0.1, 0.2, 0.4, 0.8\}$ and fixed $\sigma = 0.4$ and refer it as SHAPR.

G.2.3. LIME

Local Interpretable Model-agnostic Explanations (LIME) (Ribeiro et al., 2016) interprets individual predictions based on locally approximating the model around a given prediction. We use LIME from the official SHAP repository.

G.2.4. MAPLE

MAPLE (Plumb et al., 2018) is another technique that combines local neighborhood selection with local feature selection. We use official implementation from the official SHAP repository.

G.2.5. L2X

L2X (Chen et al., 2018b) used a mutual information-based approach to explainability. The L2X explainer has a hyperparameter k which needs to be defined by the user to decide the top k most important features to pick. For each D-dimensional data point, L2X outputs a D-dimensional binary vector I_k with 1 indicating important features and 0 indicating unimportant features. Because k is often unknown a priori, we modified L2X as follows:

$$\boldsymbol{w} = \frac{2}{k(k+1)} \sum_{k=1}^{D} I_k, \tag{7}$$

where $\frac{2}{k(k+1)}$ is a scaling factor to ensure the elements in $\boldsymbol{w}$ sum up to 1. The original L2X model uses 1 million training samples to achieve good performance, due to the computation limitation of metrics calculation, we limit the training set size of synthetic experiment to 1000, and experiments show that L2X often fails to achieve good performance.

G.2.6. RANDOM

RANDOM explainer is implemented to serve as a baseline model. The explainer generates random weights from standard normal distribution.

H. Dataset details

For 5-dimensional datasets, linear $w = [4, 3, 2, 1, 0]$,

piecewise constant:

$$\Psi_1(x_1) = \begin{cases} 1, \; x_1 >= 0 \\ -1, \; x_1 < 0 \end{cases} \tag{8}$$

$$\Psi_2(x_2) = \begin{cases} -2, \; x_2 < -0.5 \\ -1, \; -0.5 \le x_2 < 0 \\ 1, \; -0 \le x_2 < 0.5 \\ 2, \; x_2 \ge 0.5 \end{cases} \tag{9}$$

$$\Psi_3(x_3) = floor(2cos(\pi x_3)) \tag{10}$$

$$\Psi_i(x_i) = 0, \; i = 4, 5 \tag{11}$$

where $floor()$ is a rounding function that rounds a real number to the nearest integer with the lowest absolute value.

Nonlinear additive:

$$\Psi_1(x_1) = sin(x_1) \tag{12}$$
$$\Psi_2(x_2) = |x_2| \tag{13}$$
$$\Psi_3(x_3) = x_3^2 \tag{14}$$
$$\Psi_4(x_4) = e^{x_4} \tag{15}$$
$$\Psi_5(x_5) = 0. \tag{16}$$

I. Higher dimensional experiments

Two factors limit experiments with high dimensional features: *(1)* SHAPR, BF-SHAP, and the Shapley metrics evaluate a model $\Theta(2^D)$ times per datapoint, *(2)* ROAR-based metrics require retraining models $O(D)$ times which is computationally expensive. In Figures 5 and 6, we give experiments in the same setting as in Section 5, on a synthetic dataset with 100 dimensions, for all but the most computationally-intensive Shapley-based explainers.

J. Additional results

In this section, we present additional results and experimental details.

Performance across ML models We train three ML models: linear regression, decision tree, and multilayer perceptron, with a `piecewise constant` dataset and compare faith-. Figure 7 shows that as in Figure 2, explainer performance drops as features become more correlated. Most explainers perform well for linear regression up to $\rho = 0.75$. The performance of SHAP, SHAPR, and LIME remain relatively consistent across ML models. In contrast, BF-SHAP performs significantly worse on the tree model. The nearly consistent negative faith- score of MAPLE on the tree model provides additional evidence to Table 2 that in some cases, the most important feature weights MAPLE predicts tend be the least important.

Next, we compute evaluation metrics for five different explainers on the synthetic wine dataset. Note that computing these metrics accurately is not possible on the real wine dataset, as the conditional distribution is unknown. As shown in Table 3, SHAP performs well on the Shapley metrics, consistent with Table 2. Both LIME and MAPLE outperform SHAP on faith+. MAPLE achieves top performance on mono-, however, none of the explainers significantly outperform RANDOM.

Table 4 shows the time explainers take to generate explanations for 100 test datapoints. All of our experiments were run on CPUs. We report mean and standard deviation across three runs for all experiments except for Table 4. All synthetic experiments have a training size of 1000, and test size of 100.

The wine dataset contains 4898 datapoints. In Table 5, we give the mean squared error between explanations for predictions of models trained on the real vs. simulated wine dataset described in Section 5.

We conclude by presenting the comprehensive results for ten different evaluation metrics, seven different feature attribution algorithms, nine different datasets, and five different values of ρ.

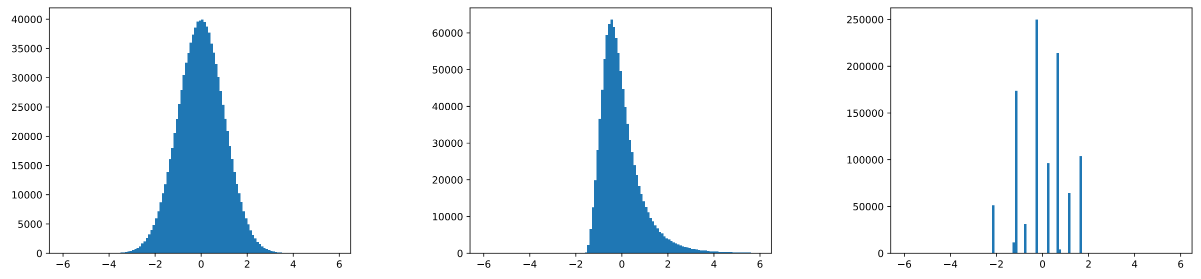

(a) (b) (c)

Figure 3. Label distribution of (a) Gaussian Linear, (b) Gaussian Nonlinear Additive, and (c) Gaussian Piecewise Constant datasets. 1 million datapoints are generated for each dataset, and 120 equal sizedd bins from -6 to 6 are used for discretizing the distribution.

Table 3. Explainer performance on the simulated wine dataset across metrics. All performance numbers are from explainers explaining a decision tree model.

	RANDOM	SHAP	LIME	MAPLE	L2X
faith- (↑)	$0.012_{\pm 0.011}$	$\mathbf{0.461}_{\pm 0.034}$	$0.237_{\pm 0.031}$	$-0.007_{\pm 0.036}$	$-0.010_{\pm 0.032}$
faith+ (↑)	$0.025_{\pm 0.038}$	$0.488_{\pm 0.023}$	$\mathbf{0.595}_{\pm 0.022}$	$0.556_{\pm 0.021}$	$0.055_{\pm 0.035}$
mono- (↑)	$0.490_{\pm 0.004}$	$0.502_{\pm 0.010}$	$0.500_{\pm 0.013}$	$\mathbf{0.506}_{\pm 0.011}$	$0.492_{\pm 0.001}$
mono+ (↑)	$0.523_{\pm 0.010}$	$\mathbf{0.556}_{\pm 0.012}$	$0.539_{\pm 0.005}$	$0.513_{\pm 0.008}$	$0.522_{\pm 0.008}$
shapley-corr (↑)	$0.011_{\pm 0.027}$	$\mathbf{0.815}_{\pm 0.024}$	$0.692_{\pm 0.019}$	$0.669_{\pm 0.007}$	$0.035_{\pm 0.055}$
shapley-mse (↓)	$1.032_{\pm 0.022}$	$\mathbf{0.014}_{\pm 0.003}$	$0.032_{\pm 0.005}$	$0.041_{\pm 0.001}$	$0.055_{\pm 0.001}$

Table 4. Time taken in seconds by explainers to explain 100 five-dimensional test datapoints from the Gaussian piecewise constant dataset for a multilayer perceptron model.

	Random	SHAP	SHAPR	BF-SHAP	MAPLE	LIME	L2X
Time (in seconds)	0.00009	3.9	323.8	0.2	3.2	28.0	6.5

Table 5. Mean squared error (MSE) between explanations for predictions of models trained on real and simulated wine dataset. Random predictions are generated from standard Gaussian distribution for every feature for each datapoint. Low MSE across ML models and explainers suggest the simulated wine dataset is a good representation of the real dataset for explainability benchmarking.

Model	SHAP	LIME	MAPLE	L2X	Random
Linear	0.028 ± 0.009	0.047 ± 0.016	0.027 ± 0.009	0.0009 ± 0.0001	
Tree	0.047 ± 0.003	0.009 ± 0.001	0.052 ± 0.012	0.0008 ± 0.0001	1.988 ± 0.001
MLP	0.028 ± 0.003	0.037 ± 0.008	0.040 ± 0.002	0.0008 ± 0.0001	

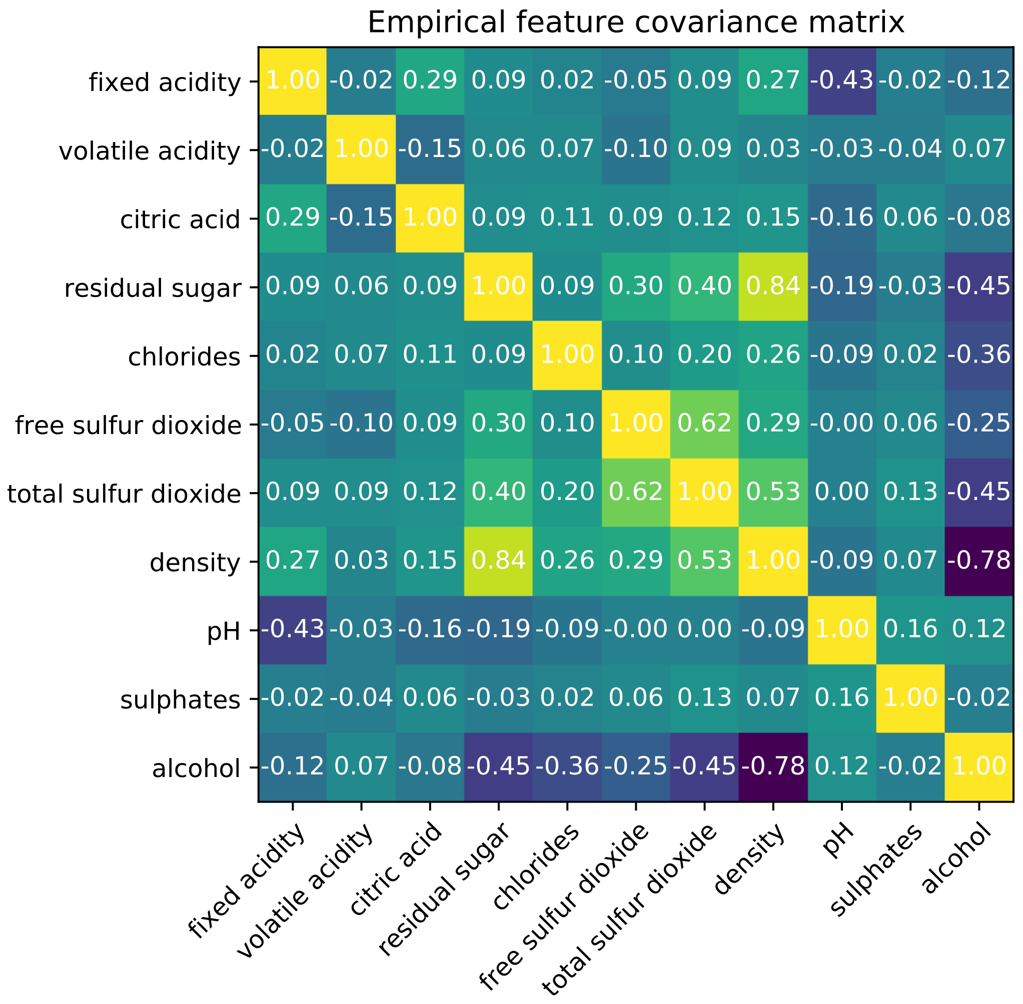

	fixed acidity	volatile acidity	citric acid	residual sugar	chlorides	free sulfur dioxide	total sulfur dioxide	density	pH	sulphates	alcohol
fixed acidity	1.00	-0.02	0.29	0.09	0.02	-0.05	0.09	0.27	-0.43	-0.02	-0.12
volatile acidity	-0.02	1.00	-0.15	0.06	0.07	-0.10	0.09	0.03	-0.03	-0.04	0.07
citric acid	0.29	-0.15	1.00	0.09	0.11	0.09	0.12	0.15	-0.16	0.06	-0.08
residual sugar	0.09	0.06	0.09	1.00	0.09	0.30	0.40	0.84	-0.19	-0.03	-0.45
chlorides	0.02	0.07	0.11	0.09	1.00	0.10	0.20	0.26	-0.09	0.02	-0.36
free sulfur dioxide	-0.05	-0.10	0.09	0.30	0.10	1.00	0.62	0.29	-0.00	0.06	-0.25
total sulfur dioxide	0.09	0.09	0.12	0.40	0.20	0.62	1.00	0.53	0.00	0.13	-0.45
density	0.27	0.03	0.15	0.84	0.26	0.29	0.53	1.00	-0.09	0.07	-0.78
pH	-0.43	-0.03	-0.16	-0.19	-0.09	-0.00	0.00	-0.09	1.00	0.16	0.12
sulphates	-0.02	-0.04	0.06	-0.03	0.02	0.06	0.13	0.07	0.16	1.00	-0.02
alcohol	-0.12	0.07	-0.08	-0.45	-0.36	-0.25	-0.45	-0.78	0.12	-0.02	1.00

Figure 4. Empirical covariance matrix of the wine dataset. Features are normalized to have unit variance and zero mean.

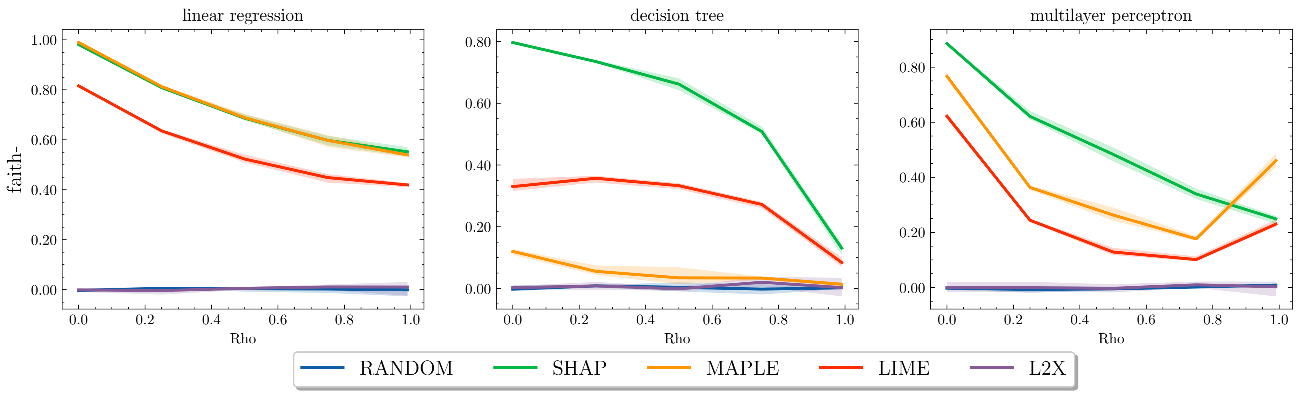

Figure 5. Results for faith- across ML models and ρs on the Gaussian linear dataset with 100 dimensions. Note that the error regions for faith- are much smaller than the error regions for mono- (Figure 6).

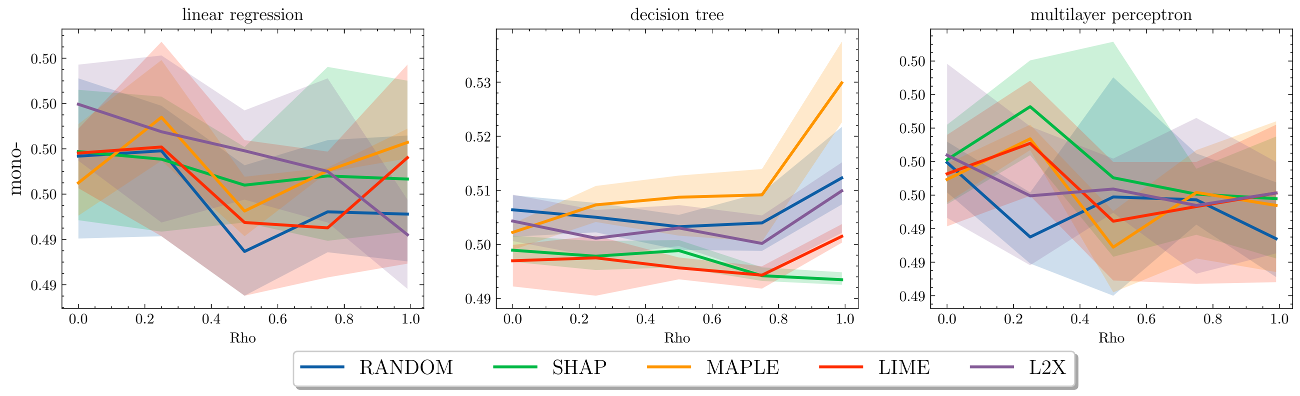

Figure 6. Results for mono- across ML models and ρs on the Gaussian linear dataset with 100 dimensions.

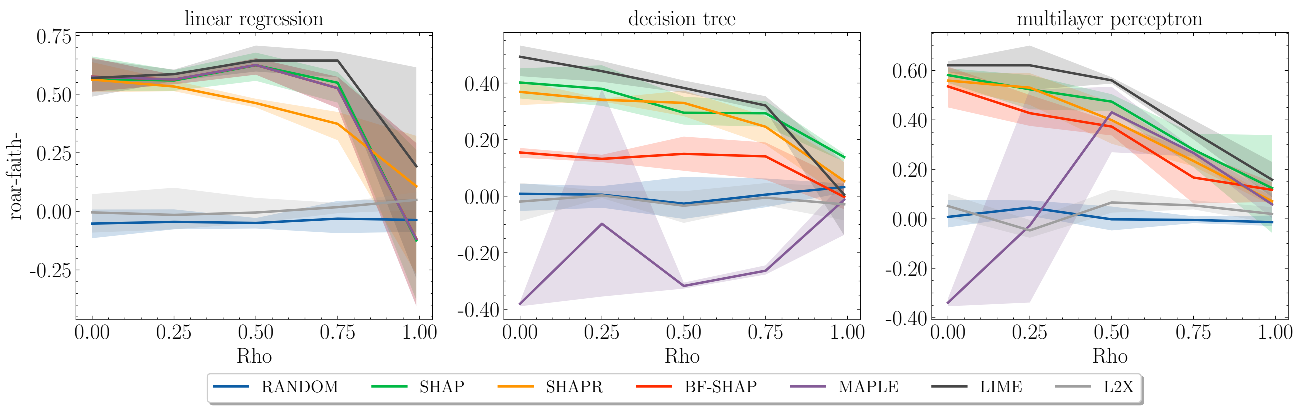

Figure 7. Results for faith- for three types of ML models– linear regression, decision tree, and multilayer perceptron– trained on a Gaussian piecewise constant dataset.

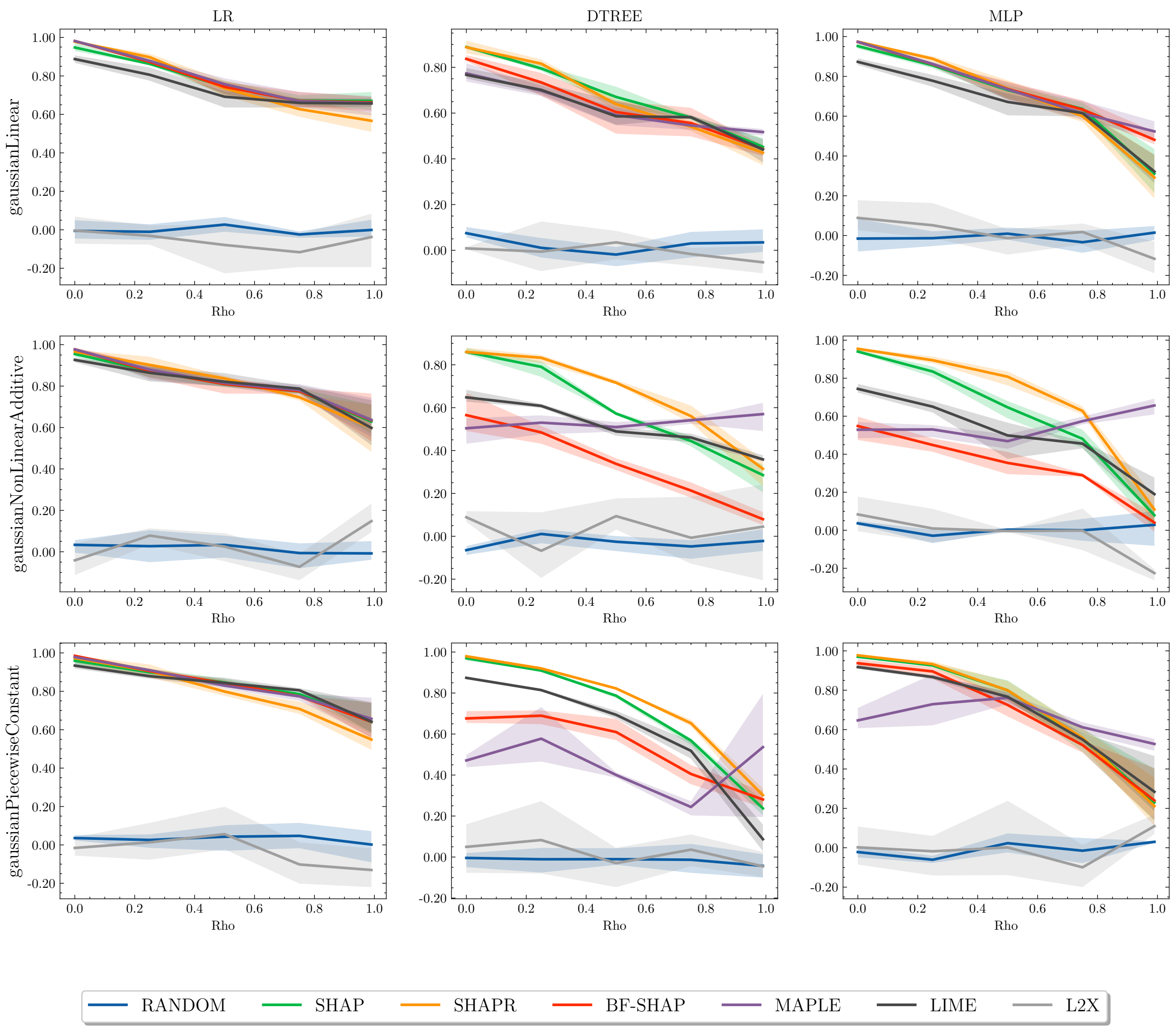

Figure 8. Results of faith- across ML models, dataset types, and ρs.

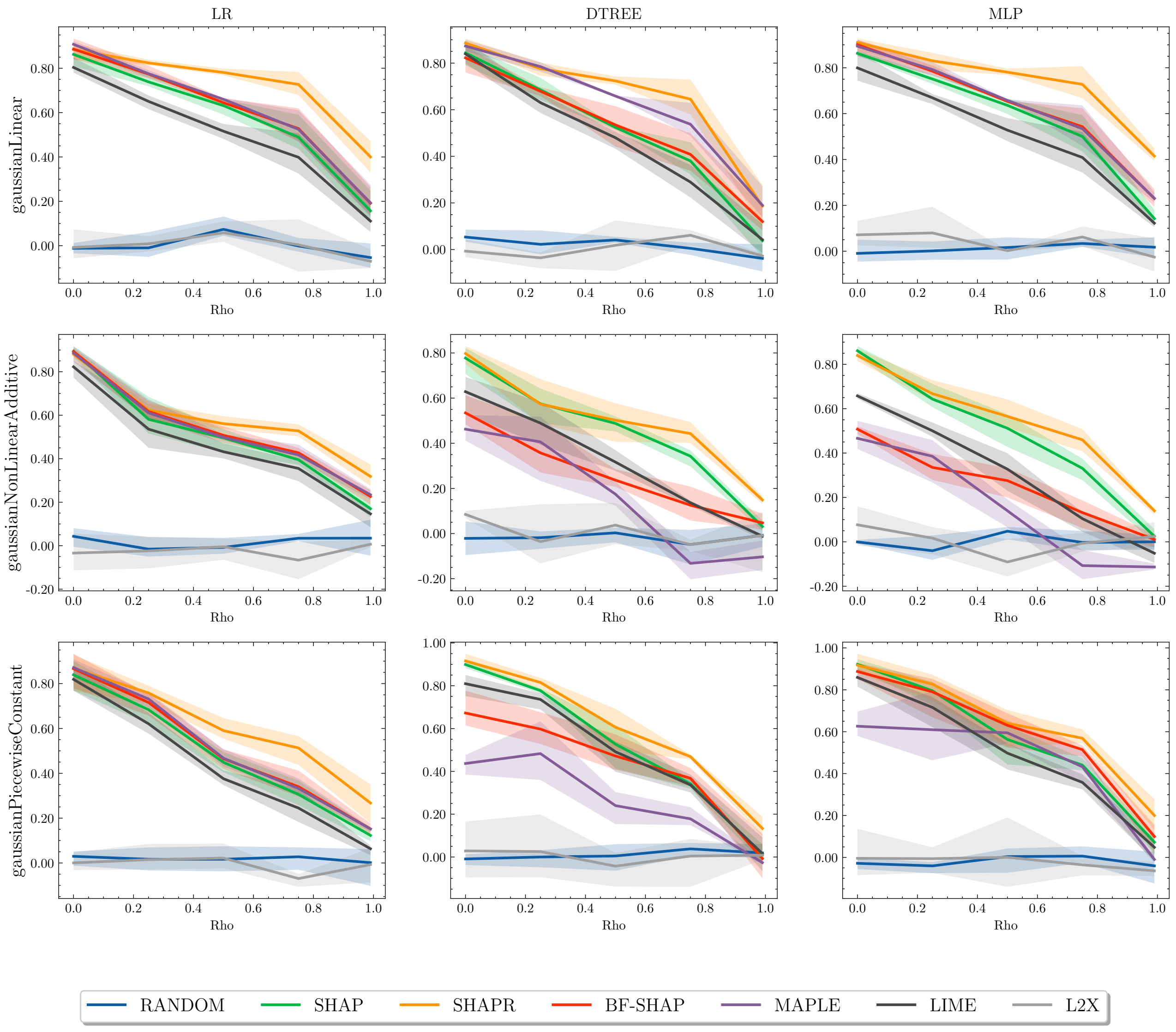

Figure 9. Results of faith+ across ML models, dataset types, and ρs.

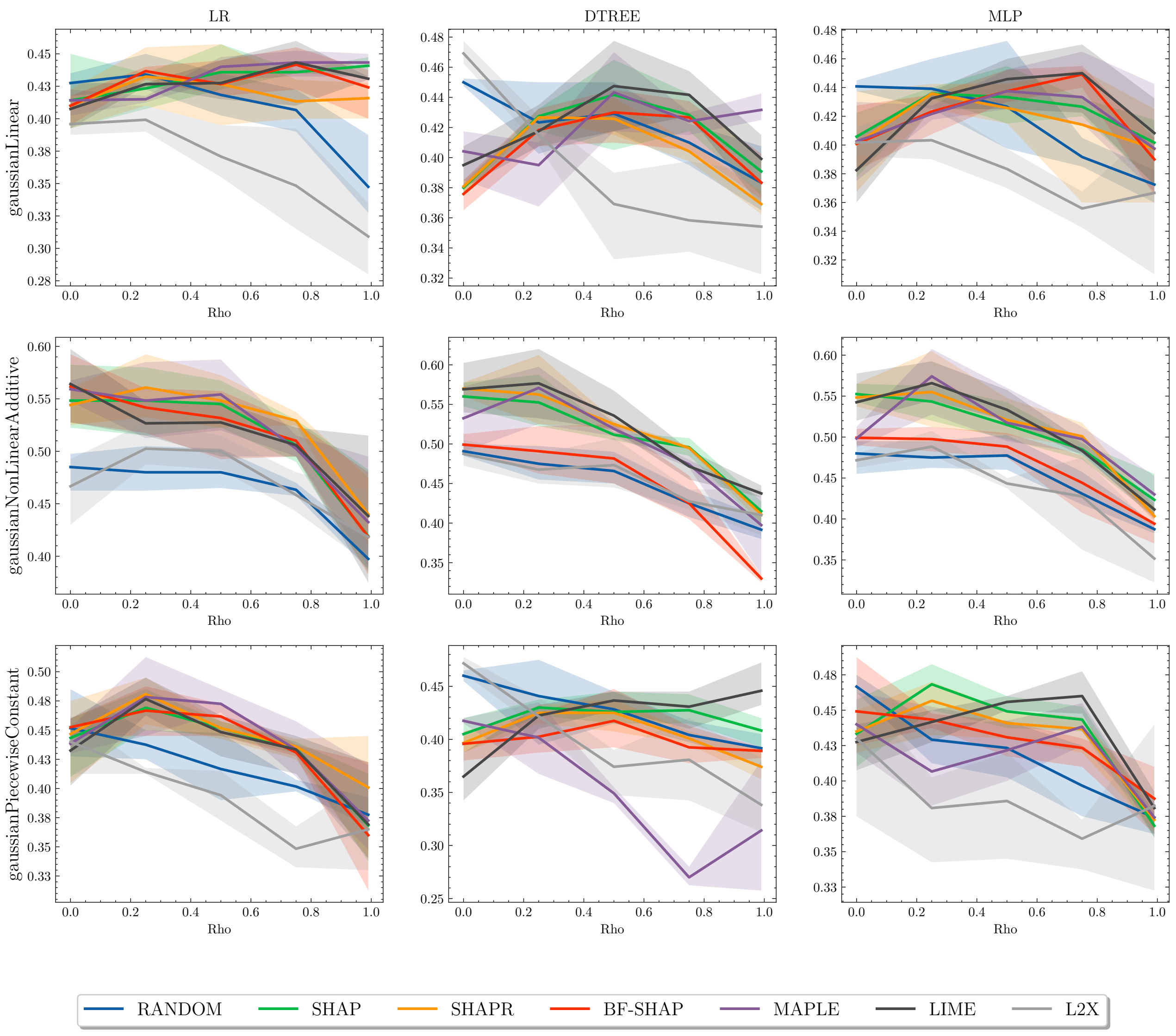

Figure 10. Results of mono- across ML models, dataset types, and ρs.

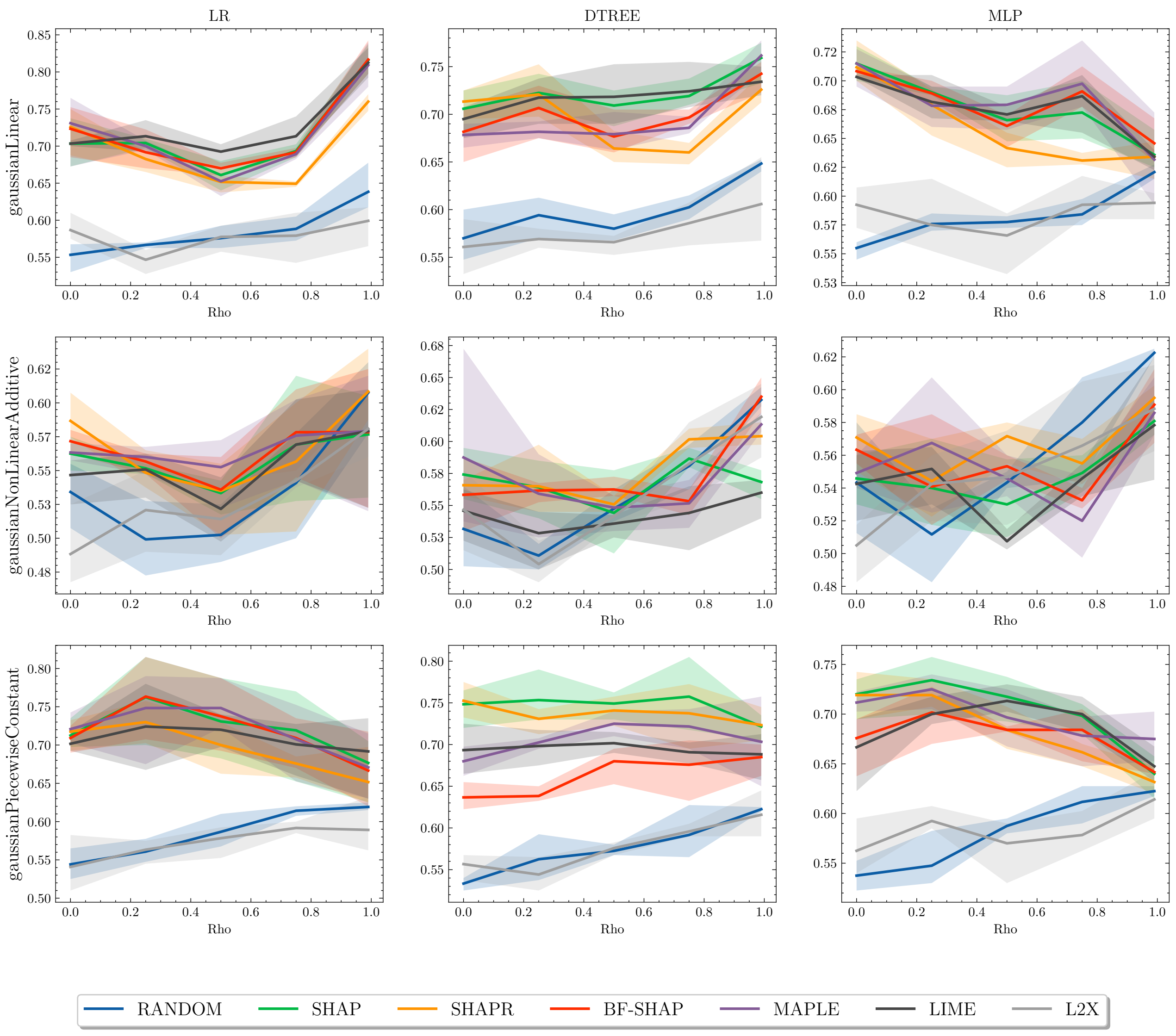

Figure 11. Results of mono+ across ML models, dataset types, and ρs.

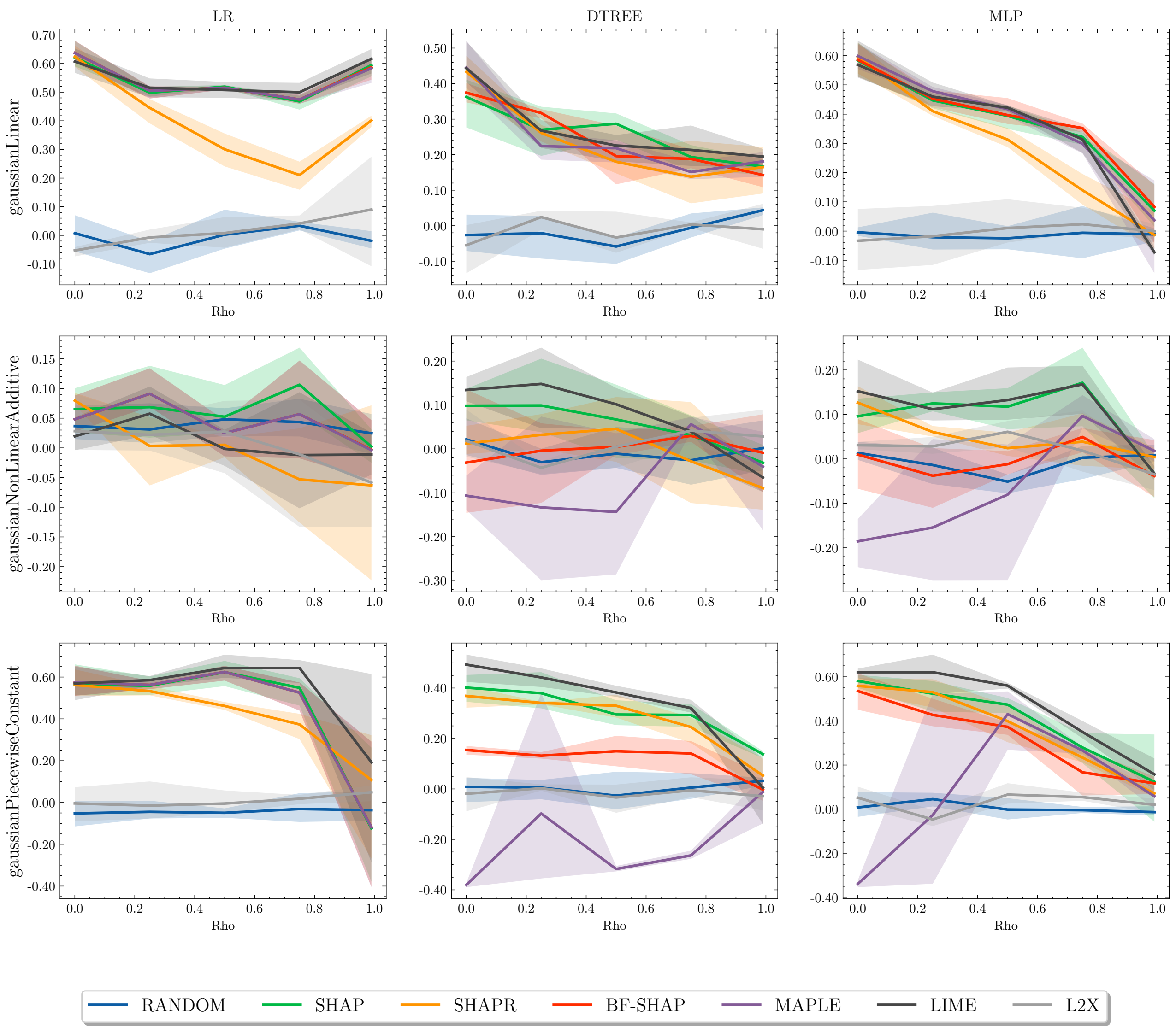

Figure 12. Results of roar-faith- across ML models, dataset types, and ρs.

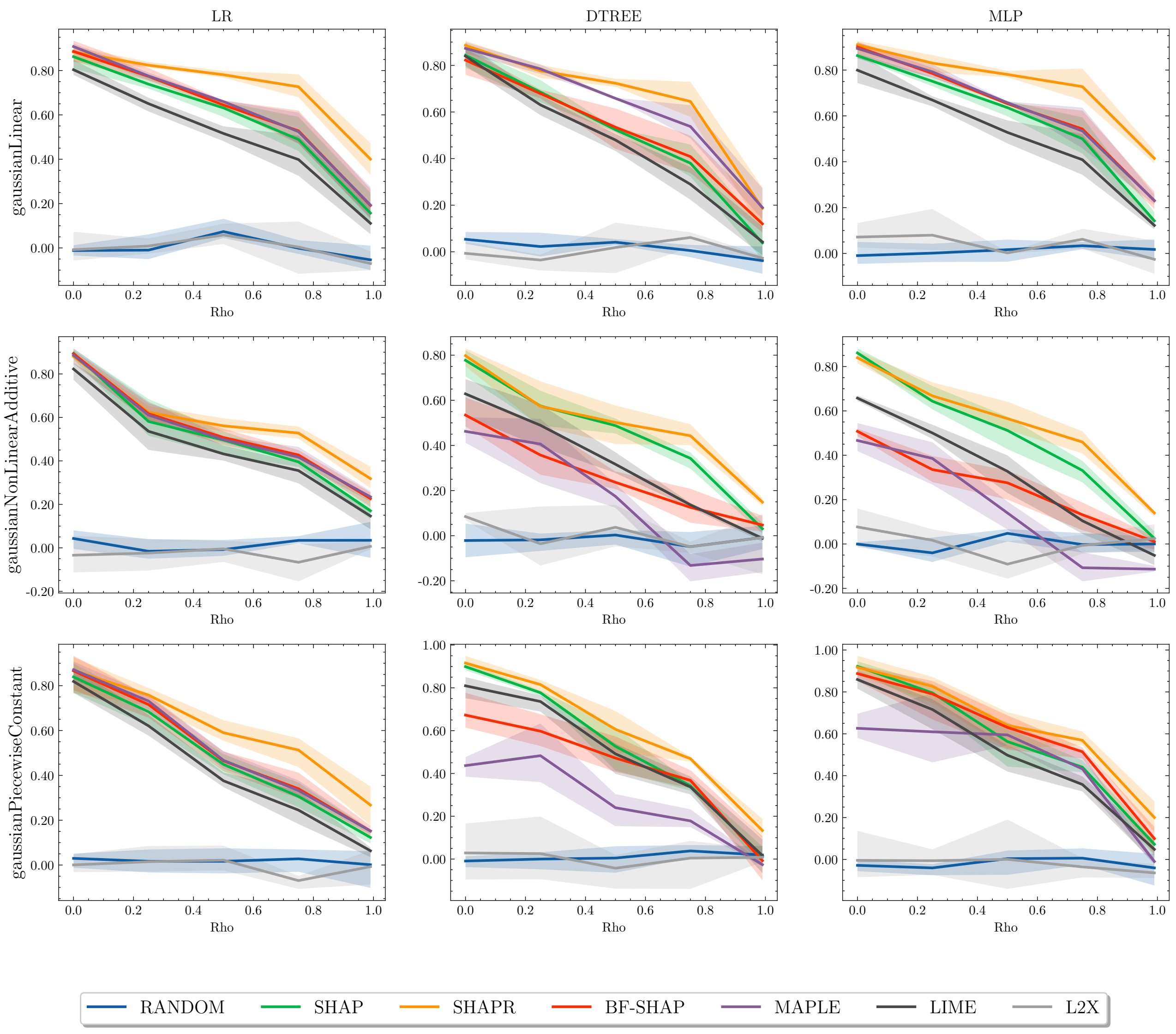

Figure 13. Results of roar-faith+ across ML models, dataset types, and ρs.

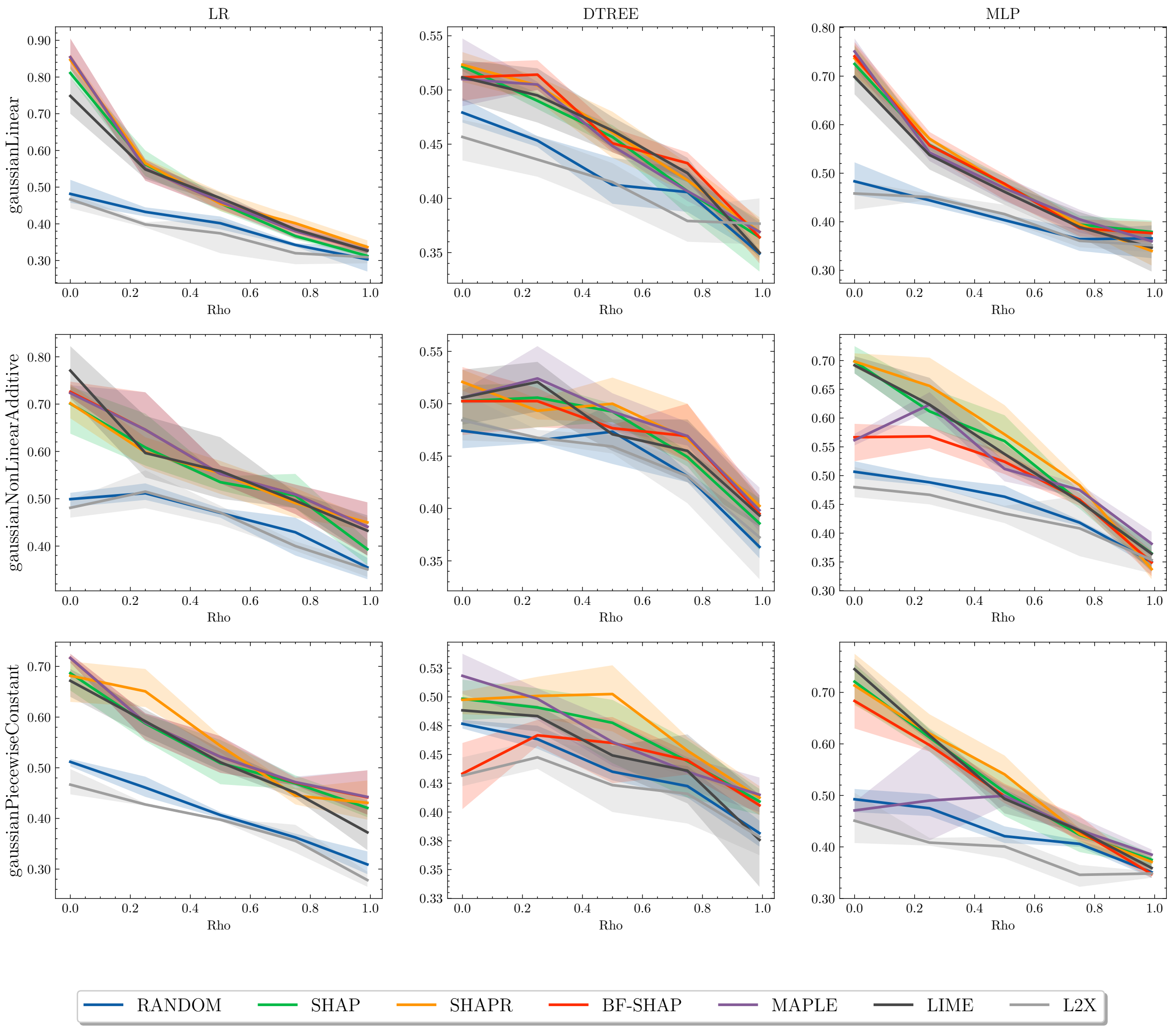

Figure 14. Results of roar-mono- across ML models, dataset types, and ρs.

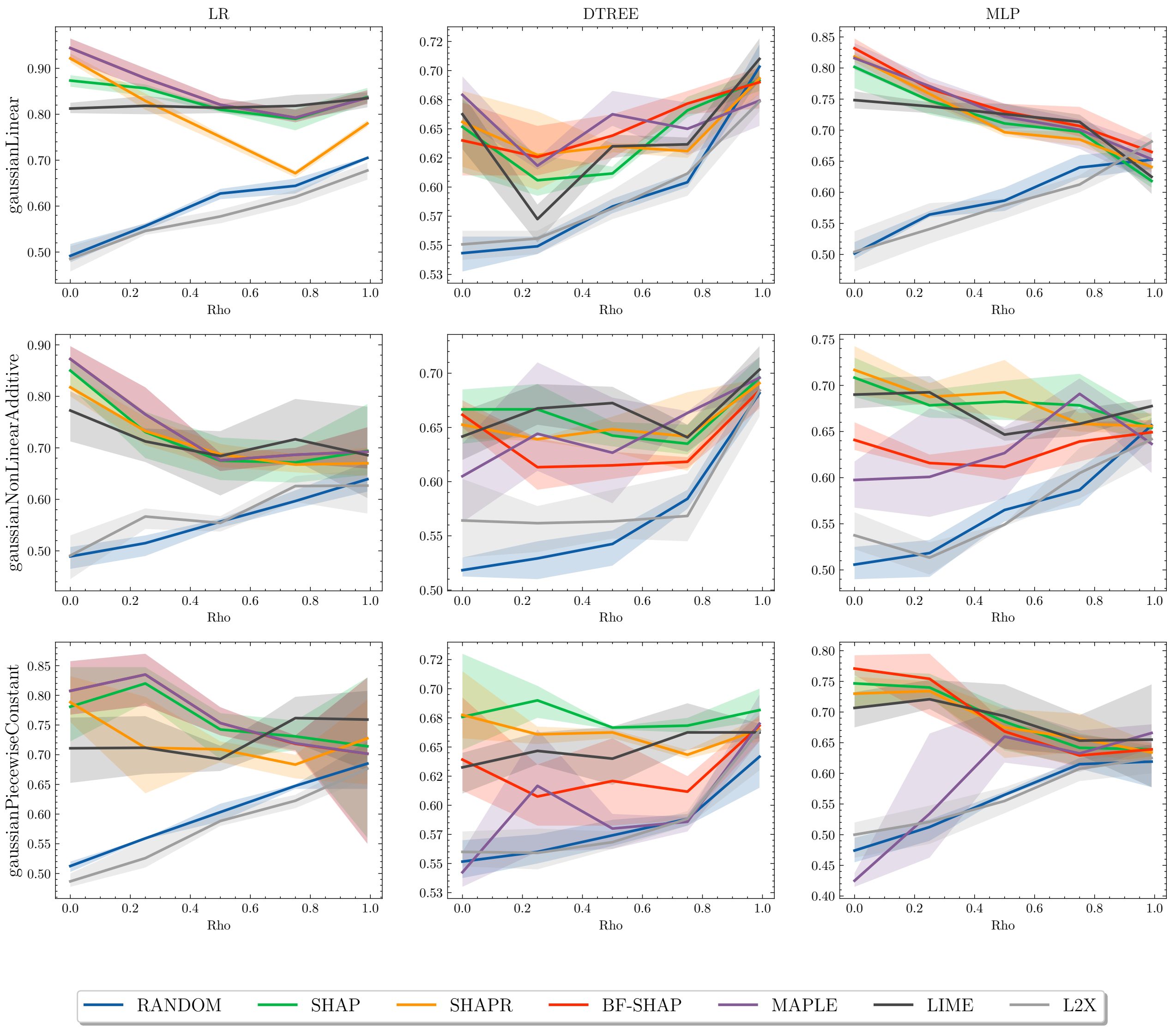

Figure 15. Results of roar-mono+ across ML models, dataset types, and ρs.

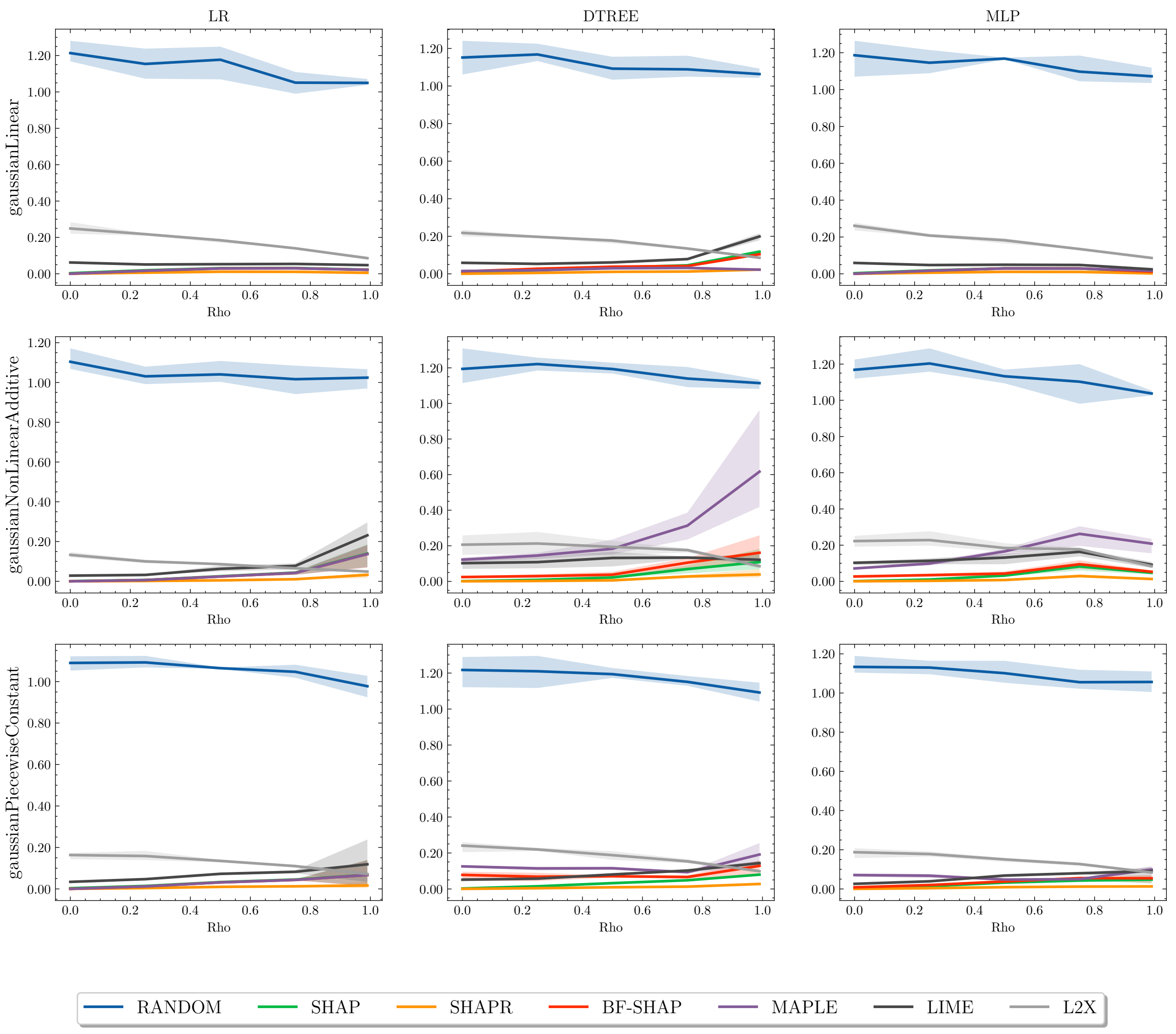

Figure 16. Results of shapley-mse across ML models, dataset types, and ρs.

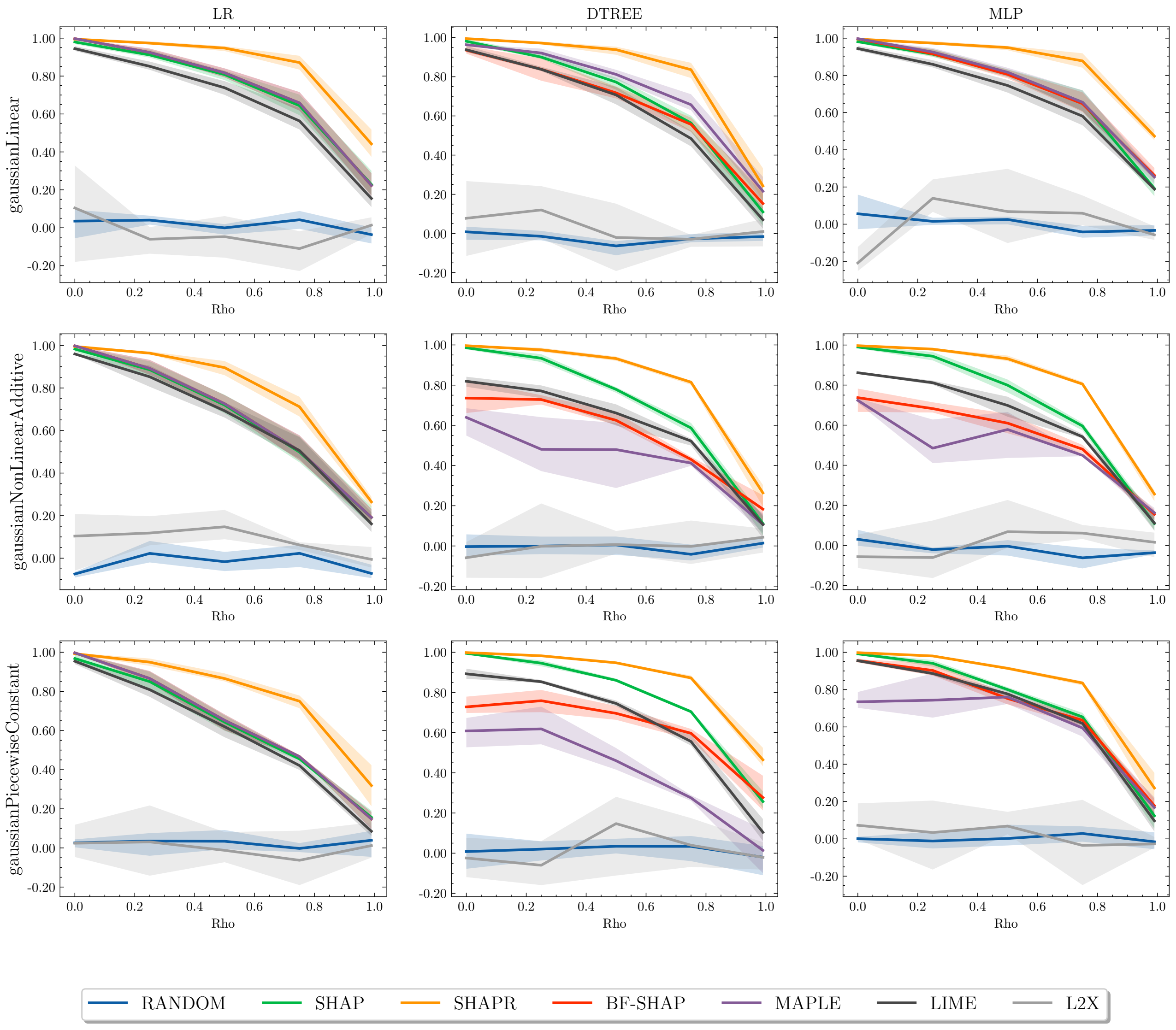

Figure 17. Results of shapley-corr across ML models, dataset types, and ρs.